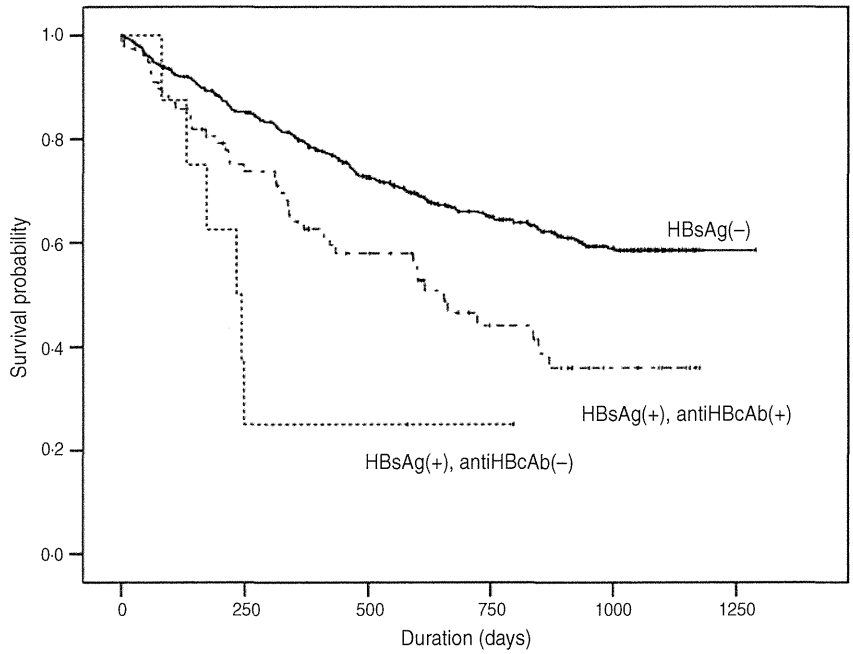


**Fig. 2.** Kaplan–Meier survival probability estimate showing that HBV co-infected individuals without anti-HBcAb had the poorest survival compared to HIV mono-infected or HBV co-infected patients with anti-HBcAb.

with HBV co-infection was independent of age, gender, transmission route, clinical symptoms and immunological status such as CD4 cell count. Nevertheless, as with most multivariate regression models, residual confounding cannot be fully ruled out. We also analysed some behavioural factors like excessive alcohol consumption. However, we did not find any significant association with HBV co-infection.

It is striking that HBV co-infected patients without anti-HBcAb had the poorest prognosis. Even after adjustment for demographic and clinical factors, the impact on death remained substantially high. Avettand-Fenoel *et al.* suggested three circumstances leading to failure to elicit anti-HBcAb during HBV infection [25]. Our patients may fit two of these circumstances. First, the majority of HBV patients in developing countries were vertically infected. It is hypothesized that infants born to HBeAg-positive carrier mothers may result in the lack of anti-HBcAb production as they have helper T-cell tolerance to HBV core Ag and HBeAg induced by transplacental maternal HBVAg. Another reason for lack of anti-HBcAb production is due to immunocompromised condition like uncontrolled HIV infection. If the former circumstance is true, these patients should be HBVe Ag-positive but such data is not available in this study. Clinical implication of the absence of anti-HBcAb during chronic HBV infection remain largely unknown except that it is not linked to severe hepatic disease course [26] although its impact on HIV progression has never been reported. We found that the frequency of HBV patients without anti-HBcAb is not uncommon in our HIV-infected population. Together with the poor prognosis, our observation suggests that more attention should be given to this group. However, the results should be interpreted with caution because of the small number of HBV patients without anti-HBcAb.

After the initiation of HAART, in both wealthy and resource-limited countries, the proportion of liver-related mortality increased in hepatitis and HIV co-infected patients [27–30]. Unfortunately, adequate treatment for chronic hepatitis is not available in resource-limited countries. A tenofovir-based first-line regimen is now recommended by WHO and is being adopted in many countries. However, the price of tenofovir needs to fall to allow more widespread access to this drug. Currently, the prevailing regimen for chronic hepatitis infection includes lamivudine alone in the most resource-limited countries. Thus, most HIV patients with HBV co-infection are inevitably receiving lamivudine monotherapy for HBV infection. The choice of antiretrovirals for such patients should include at least two drugs effective against HBV such as tenofovir. Last, screening for hepatitis co-infection at the same time as HIV diagnosis should be urgently implemented.

Table 3 (*b*). *Impact of HBs Ag and anti-HBc Ab status on survival*

| Variables | HR (95% CI) | *P* value | aHR (95% CI) | *P* value |
|---|---|---|---|---|
| Male sex | 2·59 (2·02–3·33) | <0·001 | 1·23 (0·96–1·63) | 0·11 |
| Age <35 years* | 0·79 (0·61–1·01) | 0·06 | 0·79 (0·61–1·02) | 0·08 |
| Previous ART† | 0·67 (0·49–0·92) | 0·01 | 1·10 (0·79–1·53) | 0·59 |
| Transmission mode | | | | |
| IDU | Ref. | — | — | — |
| Homosexual | 0·36 (0·05–2·58) | 0·31 | — | — |
| Heterosexual | 0·68 (0·17–2·72) | 0·58 | — | — |
| Others | 1·12 (0·21–6·13) | 0·89 | — | — |
| Clinical symptom*‡ | | | | |
| Asymptomatic | Ref. | | Ref. | — |
| Symptomatic, non AIDS | 3·06 (2·16–4·33) | <0·001 | 1·47 (1·10–2·15) | 0·05 |
| AIDS, symptomatic | 6·65 (4·93–8·98) | <0·001 | 2·03 (1·42–2·90) | <0·001 |
| Baseline CD4 cell count† (cells/$\mu$l) | | | | |
| ⩾200 | Ref. | — | Ref. | — |
| 50–199 | 4·46 (2·91–6·84) | <0·001 | 2·03 (1·42–2·90) | <0·001 |
| <50 | 12·7 (8·72–18·6) | <0·001 | 6·34 (3·99–10·3) | <0·001 |
| Baseline viral load (copies/ml) | | | | |
| <10000 | Ref. | — | Ref. | — |
| 10000–49999 | 2·44 (1·04–5·75) | 0·04 | 1·73 (0·72–4·13) | 0·22 |
| 50000–99999 | 3·30 (1·39–7·85) | 0·007 | 1·17 (0·47–2·93) | 0·74 |
| ⩾100000 | 8·79 (4·13–18·7) | <0·001 | 2·09 (0·91–4·78) | 0·08 |
| Baseline platelet count | | | | |
| <150000 | 1·52 (1·00–2·29) | 0·05 | 1·28 (0·84–1·94) | 0·25 |
| HBV serology | | | | |
| HBsAg(–) | Ref. | — | Ref. | — |
| HBsAg(+)anti-HBcAb(–) | — | — | 6·34 (3·99–10·3) | <0·001 |
| HBsAg(+) anti-HBcAb(+) | — | — | 1·62 (1·14–2·29) | 0·007 |

IQR, Interquartile range; ART, antiretroviral therapy; AIDS, acquired immunodeficiency syndrome; HR, hazard ratio; aHR, adjusted hazard ratio; CI, confidence interval; HBsAg, hepatitis B surface antigen; anti-HBcAb, anti-hepatitis B core antibody.

* At the time of enrolment.

† Experience with antiretroviral therapy is limited to mono- or dual-therapy.

‡ Definition of AIDS according to the National guidelines for the clinical management of HIV infection in children and adults, 6th edn. Thailand: Ministry of Public Health, 2000.

In summary, whereas HCV co-infection showed marginal association with the survival, HBV co-infection, especially without anti-HBcAb, increased the all-cause mortality in HAART-naive HIV patients in resource-limited countries. In this setting, clinicians and healthcare providers should prioritize HIV/chronic hepatitis co-infected individuals.

## ACKNOWLEDGEMENTS

This study was funded by Japan International Co-operation Agency (JICA), a Grant from the National Center for Global Health and Medicine, Thai Ministry of Public Health and Japan Ministry of Education, Culture, Sports, Science and Technology grant-in-aids. The authors thank the Department of Medical Sciences of the Ministry of Public Health of Thailand, all of the patients enrolled in this study, Dr Somsak Thamthitiwat and staff at Lampang Hospital, especially Ms. S Kasemsuk, Ms. S. Seneewong-naayudhaya, Ms. A Suyasarojna, Mr P Wongnamnong, Ms. K Yoddumnern, Ms. K Lor-yont, Mr W. Khaewkarnka, Mr S. Umnajsirisuk and Mr S. Niyom-thai. The authors also thank Professor Jonathan Weber and Professor William Hall for their valuable comments.

## DECLARATION OF INTEREST

None.

## REFERENCES


1. **Te HS, Jensen DM.** Epidemiology of hepatitis B and C viruses: a global overview. *Clinics in Liver Disease* 2010; **14**: 1–21.
2. **Gupta S, Singh S.** Hepatitis B and C virus co-infections in human immunodeficiency virus positive North Indian patients. *World Journal of Gastroenterology* 2006; **12**: 6879–6883.
3. **Nagu TJ, Bakari M, Matee M.** Hepatitis A, B and C viral co-infections among HIV-infected adults presenting for care and treatment at Muhimbili National Hospital in Dar es Salaam, Tanzania. *BMC Public Health* 2008; **8**: 416.
4. **Sungkanuparph SVA, *et al.*** Prevalence of hepatitis B virus and hepatitis C virus co-infection with human immunodeficiency virus in Thai patients: a tertiary-care-based study. *Journal of the Medical Association of Thailand* 2004; **87**: 1349–1354.
5. **Soriano V, *et al.*** Care of HIV patients with chronic hepatitis B: updated recommendations from the HIV-Hepatitis B Virus International Panel. *AIDS* 2008; **22**: 1399–410.
6. **Puoti M, *et al.*** Natural history of chronic hepatitis B in co-infected patients. *Journal of Hepatology* 2006; **44** (1 Suppl.): S65–70.
7. **Soriano V, *et al.*** Care of patients coinfected with HIV and hepatitis C virus: 2007 updated recommendations from the HCV-HIV International Panel. *AIDS* 2007; **21**: 1073–1089.
8. **Graham CS, *et al.*** Influence of human immunodeficiency virus infection on the course of hepatitis C virus infection: a meta-analysis. *Clinical Infectious Diseases* 2001; **33**: 562–569.
9. **The Data Collection on Adverse Events of Anti-HIV Drugs Study Group.** Liver-related deaths in persons infected with the human immunodeficiency virus: the D:A:D Study. *Archives of Internal Medicine*. 2006; **166**: 1632–1641.
10. **Thompson MA, *et al.*** Antiretroviral treatment of adult HIV infection: 2010 recommendations of the International AIDS Society-USA panel. *Journal of the American Medical Association* 2010; **304**: 321–333.
11. **WHO.** Towards universal access – scaling up priority HIV/AIDS interventions in the health sector, progress report 2010. World Health Organization, 2010.
12. **Klein MB, Laronde RG, Suissa S.** The impact of hepatitis C virus coinfection on HIV progression before and after highly active antiretroviral therapy. *Journal of Acquired Immune Deficiency Syndromes* 2003; **33**: 365–372.
13. **Piroth L, *et al.*** Does hepatitis C virus co-infection accelerate clinical and immunological evolution of HIV-infected patients? *AIDS* 1998; **12**: 381–388.
14. **Ockenga J, *et al.*** Hepatitis B and C in HIV-infected patients. Prevalence and prognostic value. *Journal of Hepatology* 1997; **27**: 18–24.
15. **Nikolopoulos GK, *et al.*** Impact of hepatitis B virus infection on the progression of AIDS and mortality in HIV-infected individuals: a cohort study and meta-analysis. *Clinical Infectious Diseases* 2009; **48**: 1763–1771.
16. **Gilson RJC, *et al.*** Interactions between HIV and hepatitis B virus in homosexual men: effects on the natural history of infection. *AIDS* 1997; **11**: 597–606.
17. **Staples JCT, Rimland Dudas D.** Hepatitis C in HIV (human immunodeficiency virus), Atlanta V. A. (Veterans Affairs Medical Center) Cohort Study (HAVACS): the effect of coinfection on survival. *Clinical Infectious Diseases* 1999; **29**: 150–154.
18. **Sulkowski MS, *et al.*** Hepatitis C and progression of HIV disease. *Journal of the American Medical Association* 2002; **288**: 199–206.
19. **Greub BLG, *et al.*** Study. Clinical progression, survival, and immune recovery during antiretrovial therapy in patients with HIV-1 and hepatitis C virus co-infection: the Swiss HIV Cohort Study. *Lancet* 2000; **356**: 1800–1805.
20. **Wichukchinda N, *et al.*** TIM1 haplotype may control the disease progression to AIDS in a HIV-1-infected female cohort in Thailand. *AIDS* 2010; **24**: 1625–1631.
21. **Wichukchinda N, *et al.*** Protective effects of IL4–589 T and RANTES-28 G on HIV-1 disease progression in infected Thai females. *AIDS* 2006; **20**: 189–196.
22. **Rothenberg R, *et al.*** Survival with the acquired immunodeficiency syndrome. Experience with 5833 cases in New York City. *New England Journal of Medicine* 1987; **317**: 1297–1302.
23. **El-Serag HB, *et al.*** Survival in hepatitis C and HIV co-infection: a cohort study of hospitalized veterans. *Clinical Gastroenterology and Hepatology* 2005; **3**: 175–183.
24. **Gomez-Gonzalo M, *et al.*** The hepatitis B virus X protein induces HIV-1 replication and transcription in synergy with T-cell activation signals: functional roles of NF-kappaB/NF-AT and SP1-binding sites in the HIV-1 long terminal repeat promoter. *Journal of Biological Chemistry* 2001; **276**: 35435–35443.
25. **Avettand-Fenoel V, *et al.*** Immune suppression as the etiology of failure to detect anti-HBc antibodies in patients with chronic hepatitis B virus infection. *Journal of Clinical Microbiology* 2006; **44**: 2250–2253.
26. **Melegari M, *et al.*** Conserved core protein sequences in hepatitis B virus infected patients without anti-HBc. *Journal of Hepatology* 1991; **13**: 187–191.
27. **Hoffman CJ, *et al.*** Hepatitis B and long-term HIV outcomes in coinfected HAART recipients. *AIDS* 2009; **23**: 1881–1889.
28. **Weis N, *et al.*** Impact of Hepatitis C virus coinfection on response to highly active antiretroviral therapy and outcome in HIV-infected individuals: a nationwide cohort study. *Clinical Infectious Diseases* 2006; **42**: 1481–1487.
29. **Rosenthal E, *et al.*** Liver-related deaths in HIV-infected patients between 1995 and 2005 in the French GERMIVIC Joint Study Group Network (Mortavic 2005 study in collaboration with the Mortalite 2005 survey, ANRS EN19). *HIV Medicine* 2009; **10**: 282–289.
30. **Mocroft A, *et al.*** Is there evidence for an increase in the death rate from liver-related disease in patients with HIV? *AIDS* 2005; **19**: 2117–2125.

JVI
Journals.ASM.org

# Association of Major Histocompatibility Complex Class I Haplotypes with Disease Progression after Simian Immunodeficiency Virus Challenge in Burmese Rhesus Macaques

Takushi Nomura,[a,b] Hiroyuki Yamamoto,[a] Teiichiro Shiino,[a] Naofumi Takahashi,[a,b] Taku Nakane,[a,b] Nami Iwamoto,[a,b] Hiroshi Ishii,[a,b] Tetsuo Tsukamoto,[b] Miki Kawada,[b] Saori Matsuoka,[a] Akiko Takeda,[a] Kazutaka Terahara,[c] Yasuko Tsunetsugu-Yokota,[c] Naoko Iwata-Yoshikawa,[d] Hideki Hasegawa,[d] Tetsutaro Sata,[d] Taeko K. Naruse,[e] Akinori Kimura,[e] and Tetsuro Matano[a,b]

AIDS Research Center, National Institute of Infectious Diseases, Toyama, Shinjuku-ku, Tokyo, Japan[a]; The Institute of Medical Science, The University of Tokyo, Shirokanedai, Minato-ku, Tokyo, Japan[b]; Department of Immunology, National Institute of Infectious Diseases, Toyama, Shinjuku-ku, Tokyo, Japan[c]; Department of Pathology, National Institute of Infectious Diseases, Toyama, Shinjuku-ku, Tokyo, Japan[d]; and Department of Molecular Pathogenesis, Medical Research Institute, Tokyo Medical and Dental University, Kandasurugadai, Chiyoda-ku, Tokyo, Japan[e]

**Nonhuman primate AIDS models are essential for the analysis of AIDS pathogenesis and the evaluation of vaccine efficacy. Multiple studies on human immunodeficiency virus and simian immunodeficiency virus (SIV) infection have indicated the association of major histocompatibility complex class I (MHC-I) genotypes with rapid or slow AIDS progression. The accumulation of macaque groups that share not only a single MHC-I allele but also an MHC-I haplotype consisting of multiple polymorphic MHC-I loci would greatly contribute to the progress of AIDS research. Here, we investigated SIVmac239 infections in four groups of Burmese rhesus macaques sharing individual MHC-I haplotypes, referred to as A, E, B, and J. Out of 20 macaques belonging to $A^+$ ($n = 6$), $E^+$ ($n = 6$), $B^+$ ($n = 4$), and $J^+$ ($n = 4$) groups, 18 showed persistent viremia. Fifteen of them developed AIDS in 0.5 to 4 years, with the remaining three at 1 or 2 years under observation. $A^+$ animals, including two controllers, showed slower disease progression, whereas $J^+$ animals exhibited rapid progression. $E^+$ and $B^+$ animals showed intermediate plasma viral loads and survival periods. Gag-specific $CD8^+$ T-cell responses were efficiently induced in $A^+$ animals, while Nef-specific $CD8^+$ T-cell responses were in $A^+$, $E^+$, and $B^+$ animals. Multiple comparisons among these groups revealed significant differences in survival periods, peripheral $CD4^+$ T-cell decline, and SIV-specific $CD4^+$ T-cell polyfunctionality in the chronic phase. This study indicates the association of MHC-I haplotypes with AIDS progression and presents an AIDS model facilitating the analysis of virus-host immune interaction.**

Virus-specific $CD8^+$ cytotoxic T lymphocytes (CTLs) are major effectors against persistent virus infections (13, 44). In virus-infected cells, viral antigen-derived peptides (epitopes) are bound to major histocompatibility complex class I (MHC-I) molecules and presented on the cell surface. Viral peptide-specific CTLs recognize the peptide-MHC-I complexes by their T-cell receptors. CTL effectors deliver cell death via apoptosis as well as lysis (15, 48).

Human immunodeficiency virus type 1 (HIV-1) infection induces persistent viral replication leading to AIDS progression. CTL responses play a central role in the suppression of HIV-1 replication (6, 18, 25, 32, 43). Multiple studies on HIV-1-infected individuals have shown an association of HLA genotypes with rapid or delayed AIDS progression (14, 23, 27, 51, 54). For instance, HIV-1-infected individuals possessing *HLA-B*57* tend to show a better prognosis with lower viral loads, implicating HLA-B*57-restricted epitope-specific CTL responses in this viral control (3, 33, 34). In contrast, the association of *HLA-B*35* with rapid disease progression has been indicated (8).

Nonhuman primate AIDS models are important for the analysis of AIDS pathogenesis and the evaluation of vaccine efficacy (5, 35, 47). Models of simian immunodeficiency virus (SIV) infection in macaques are widely used currently (12, 22). Indian rhesus macaques possessing certain MHC-I alleles, such as *Mamu-A*01*, *Mamu-B*08*, and *Mamu-B*17*, tend to show lower set point plasma viral loads in SIV infection (30, 36, 37, 59). Regarding MHC-I alleles, humans have a single polymorphic HLA-A, HLA-B, and HLA-C locus per chromosome, whereas MHC-I haplotypes in macaques have variable numbers of expressed polymorphic MHC-I loci (7, 9, 26, 41). Thus, the accumulation of multiple macaque groups, each sharing a different MHC-I haplotype, would contribute to the precise analysis of SIV infection.

We have been working on the establishment of an AIDS model using Burmese rhesus macaques sharing MHC-I haplotypes (38, 50). In the present study, we have focused on SIV infection in four groups of Burmese rhesus macaques, each consisting of four or more animals. These groups share MHC-I haplotypes *90-120-Ia* (referred to as A), *90-010-Ie* (E), *90-120-Ib* (B), and *90-088-Ij* (J), respectively. The analysis of SIVmac239 infection among these groups revealed differences in plasma viral loads, peripheral $CD4^+$ T cell counts, survival periods, virus-specific CTL responses, and T-cell polyfunctionality. Our results indicate the association of MHC-I haplotypes with disease progression in SIV infection and present a sophisticated model of SIV infection.

Received 11 December 2011 Accepted 27 March 2012
Published ahead of print 4 April 2012
Address correspondence to Tetsuro Matano, tmatano@nih.go.jp.

doi:10.1128/JVI.07077-11

TABLE 1 MHC-I haplotypes

| MHC-I haplotype | Confirmed MHC-I allele(s) | |
|---|---|---|
| | *Mamu-A* | *Mamu-B* |
| A (*90-120-Ia*) | *A1*043:01, A1*065:01* | *B*061:03, B*068:04, B*089:01* |
| E (*90-010-Ie*) | *A1*066:01* | *B*005:02, B*015:04* |
| B (*90-120-Ib*) | *A1*018:08, A2*005:31* | *B*036:03, B*037:01, B*043:01, B*162:01* |
| J (*90-088-Ij*) | *A1*008:01* | *B*007:02, B*039:01* |

## MATERIALS AND METHODS

**Animal experiments.** We examined SIV infections in four groups of Burmese rhesus macaques having MHC-I haplotypes *90-120-Ia* (A) ($n$ = 6), *90-010-Ie* (E) ($n$ = 6), *90-120-Ib* (B) ($n$ = 4), and *90-088-Ij* (J) ($n$ = 4). Macaques R02-007, R06-037, R07-001, R07-004, R07-009, R01-011, R06-038, R06-001, R02-004, R04-014, and R06-022, which were used as controls in previous experiments (49, 53, 58), were included in the present study. The determination of MHC-I haplotypes was based on the family study in combination with the reference strand-mediated conformation analysis (RSCA) of *Mamu-A* and *Mamu-B* genes as described previously (31). Briefly, locus-specific reverse transcription-PCR (RT-PCR) products from total cellular RNAs were prepared and used to form heteroduplex DNAs with a 5′ Cy5-labeled reference strand (50). The heteroduplex DNAs were subjected to a 6% nondenaturing acrylamide gel electrophoresis to identify the patterns of MHC-I haplotypes. In addition, although recombination events could not be ruled out, major *Mamu-A* and *Mamu-B* alleles were determined by cloning the RT-PCR products and sequencing at least 48 clones for each locus from each subject as described previously (38). Because we used locus-specific primers in the RT-PCR, which were designed on the basis of known alleles (31, 38), MHC class I alleles harboring mismatches with the primer sequences or alleles of low expression would not be amplified well, hence there was a limitation that not all of the MHC class I alleles could be detected in our study. Confirmed *Mamu-A* and *Mamu-B* alleles in MHC-I haplotypes A, E, B, and

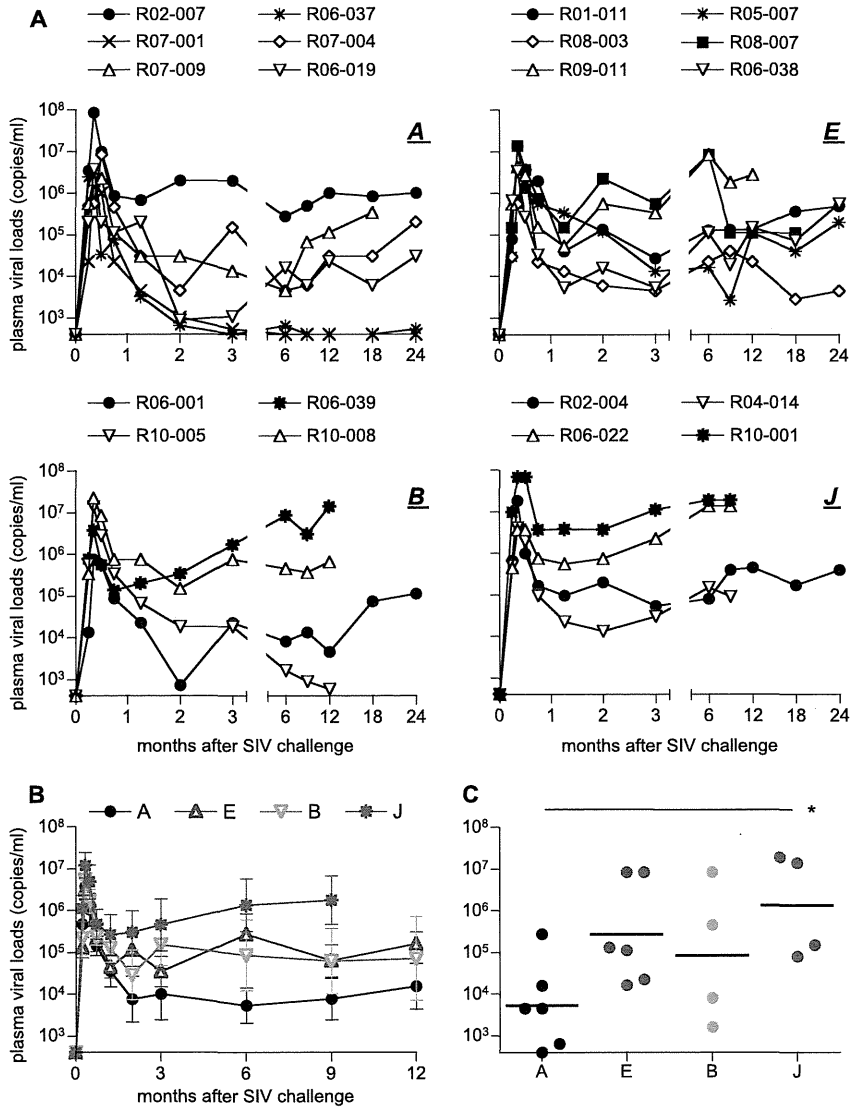


FIG 1 Plasma viral loads after SIVmac239 challenge. Plasma viral loads (SIV *gag* RNA copies/ml plasma) were determined as described previously (31). The lower limit of detection is approximately $4 \times 10^2$ copies/ml. (A) Changes in plasma viral loads after challenge in $A^+$ (upper left), $E^+$ (upper right), $B^+$ (lower left), and $J^+$ (lower right) macaques. (B) Changes in geometric means of plasma viral loads after challenge in $A^+$ (black), $E^+$ (blue), $B^+$ (green), and $J^+$ (red) animals. (C) Comparison of plasma viral loads at 6 months among four groups. Those of $A^+$ animals were significantly lower than those of $J^+$ animals ($P$ = 0.0444 by one-way ANOVA and Tukey-Kramer's multiple-comparison test).

J are shown in Table 1 (38). All animals were unvaccinated and challenged intravenously with 1,000 $TCID_{50}$ (50% tissue culture infective doses) of SIVmac239 (22). At 1 week after challenge, macaques R06-019, R06-038, and R10-008 were intravenously infused with 300 mg of nonspecific immunoglobulin G purified from uninfected rhesus macaques (57). Fifteen animals were euthanized when they showed typical signs of AIDS, such as reduction in peripheral $CD4^+$ T-cell counts, loss of body weight, diarrhea, and general weakness. Autopsy revealed lymphoatrophy or postpersistent generalized lymphadenopathy conditions consistent with AIDS (20). All animals were maintained in accordance with the guidelines for animal experiments at the National Institute of Biomedical Innovation and National Institute of Infectious Diseases.

**Analysis of SIV antigen-specific $CD8^+$ T-cell responses.** SIV antigen-specific $CD8^+$ T-cell responses were measured by the flow-cytometric analysis of gamma interferon (IFN-γ) induction as described previously (17). Peripheral blood mononuclear cells (PBMCs) were cocultured with autologous herpesvirus papioimmortalized B-lymphoblastoid cell lines (B-LCLs) pulsed with peptide pools using panels of overlapping peptides spanning the entire SIVmac239 Gag, Pol, Vif, Vpx, Vpr, Tat, Rev, Env, and Nef amino acid sequences. Intracellular IFN-γ staining was performed using a Cytofix Cytoperm kit (BD, Tokyo, Japan). Fluorescein isothiocyanate-conjugated anti-human CD4 (BD), peridinin chlorophyll protein (PerCP)-conjugated anti-human CD8 (BD), allophycocyanin Cy7 (APC-Cy7)-conjugated anti-human CD3 (BD), and phycoerythrin (PE)-conjugated anti-human IFN-γ antibodies (Biolegend, San Diego, CA) were used. Specific T-cell levels were calculated by subtracting nonspecific IFN-$\gamma^+$ T-cell frequencies from those after peptide-specific stimulation. Specific T-cell levels of less than 100 cells per million PBMCs were considered negative. Using PBMCs obtained from four SIV-infected macaques, we compared antigen-specific $CD8^+$ T-cell frequencies measured by this method (using peptide-pulsed B-LCLs) to those measured by the flow-cytometric analysis of IFN-γ induction after a pulse of PBMCs with peptides (without using B-LCLs). The levels of the former tended to be slightly higher than those of the latter. Specific $CD8^+$ T-cell responses, which were shown to be 100 to 200 cells per million PBMCs by the former method using B-LCLs, were undetectable by the latter method.

**Sequencing analysis of plasma viral genomes.** Viral RNAs were extracted using the High Pure Viral RNA kit (Roche Diagnostics, Tokyo, Japan) from macaque plasma obtained around 1 year after challenge. Fragments of cDNAs encoding SIVmac239 Gag, Pol, Vif, Vpx, Vpr, Tat, Rev, and Nef were amplified by nested RT-PCR from plasma RNAs and subjected to direct sequencing by using dye terminator chemistry and an automated DNA sequencer (Applied Biosystems, Tokyo, Japan) as described before (19). Predominant nonsynonymous mutations were determined. The Env-coding region, which is known to have multiple antibody-related mutations, was not included for the analysis.

**Analysis of SIV-specific polyfunctional T-cell responses.** To analyze polyfunctionality in SIV-specific T-cell responses, we examined the SIV-specific induction of IFN-γ, tumor necrosis factor alpha (TNF-α), interleukin-2 (IL-2), macrophage inflammatory protein 1β (MIP-1β), and CD107a in $CD4^+$ and $CD8^+$ T cells as described previously (58), with some modifications. Around 8 months after challenge, PBMCs were cocultured with B-LCLs infected with vesicular stomatitis virus G protein-pseudotyped SIVGP1 for the SIV-specific stimulation or mock-infected B-LCLs for nonspecific stimulation. The pseudotyped virus was obtained by the cotransfection of 293T cells with a vesicular stomatitis virus G protein expression plasmid and an *env* and *nef* deletion-containing simian-human immunodeficiency virus molecular clone (SIVGP1) DNA that has the genes encoding SIVmac239 Gag, Pol, Vif, Vpx, and a part of Vpr (31, 46). Immunostaining was performed using a Fix & Perm fixation and permeabilization kit (Invitrogen, Tokyo, Japan) and the following monoclonal antibodies: APC-Cy7-conjugated anti-human CD3 (BD), PE-Texas red-conjugated anti-human CD4 (Invitrogen), Alexa Fluor 700-conjugated anti-human CD8 (BD), PE-Cy7-conjugated anti-human IFN-γ (eBioscience, San Diego, CA), Pacific blue-conjugated anti-human TNF-α (Biolegend), PerCP-Cy5.5-conjugated anti-human IL-2 (Biolegend), PE-conjugated anti-human MIP-1β (BD), and Alexa Fluor 647-conjugated anti-human CD107a (Biolegend). Dead cells were stained using Live/Dead Fixable Dead Cell Stain kit (Invitrogen). Analysis was carried out using PESTLE (version 1.6.1) and SPICE (version 5.2) programs as described previously (42). The polyfunctionality (polyfunctional value) was shown as mean numbers of induced factors among the five (IFN-γ, TNF-α, IL-2, MIP-1β, and CD107a) per SIV-specific T cell.

**Statistical analysis.** Statistical analyses were performed using R software (R Development Core Team). Comparisons were performed by one-way analysis of variance (ANOVA) and Tukey-Kramer's multiple comparison test with significance levels set at $P < 0.05$. Correlation was analyzed by the Pearson test.

TABLE 2 List of macaques in this study

| MHC-I haplotype | Macaque | Disease progression | Euthanasia time point (mo) |
|---|---|---|---|
| A | R02-007 | AIDS | 42 |
| A | R06-037 | No | 49 |
| A | R07-001 | No | 49 |
| A | R07-004 | AIDS | 40 |
| A | R07-009 | AIDS | 17 |
| A | R06-019 | AIDS | 43 |
| E | R01-011 | AIDS | 24 |
| E | R05-007 | AIDS | 37 |
| E | R08-003 | Under observation (24 months) | |
| E | R08-007 | AIDS | 20 |
| E | R09-011 | AIDS | 12 |
| E | R06-038 | AIDS | 22 |
| B | R06-001 | AIDS | 34 |
| B | R06-039 | AIDS | 13 |
| B | R10-005 | Under observation (12 months) | |
| B | R10-008 | Under observation (12 months) | |
| J | R02-004 | AIDS | 37 |
| J | R04-014 | AIDS | 9 |
| J | R06-022 | AIDS | 5 |
| J | R10-001 | AIDS | 9 |

## RESULTS

**SIV infection in Burmese rhesus macaques.** We accumulated four groups of unvaccinated, SIVmac239-infected Burmese rhesus macaques, groups $A^+$ ($n = 6$), $E^+$ ($n = 6$), $B^+$ ($n = 4$), and $J^+$ ($n = 4$), sharing MHC-I haplotypes A (*90-120-Ia*), E (*90-010-Ie*), B (*90-120-Ib*), and J (*90-088-Ij*), respectively, to compare SIV infections among these groups (Table 1). Out of these 20 animals, 18 showed persistent viremia (geometric mean plasma viral loads at 6 months of $1.6 \times 10^5$ copies/ml), while in the remaining two ($A^+$ macaques R06-037 and R07-001), plasma viral loads became less than $10^3$ copies/ml or were undetectable at the set point (Fig. 1A). The former 18 animals are referred to as noncontrollers and the latter two as controllers in this study. Fifteen noncontrollers were euthanized with AIDS progression in 4 years (geometric mean survival period of 24 months), and the remaining three, after 1 or 2 years, are under observation (Table 2).

Group $A^+$ macaques, including two controllers, showed lower set point viral loads, whereas group $J^+$ macaques had higher viral loads (Fig. 1B). Viral loads in group $E^+$ and $B^+$ macaques were at intermediate levels. Multiple comparisons indicated significant

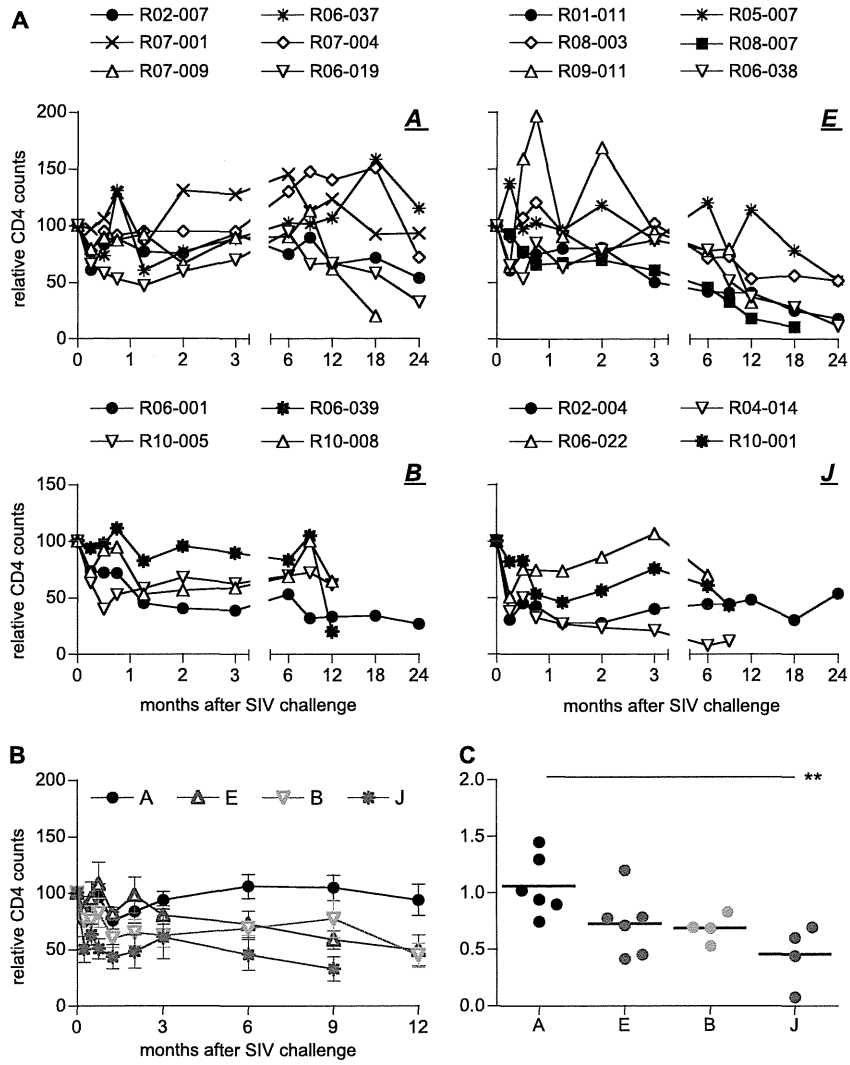


FIG 2 Relative CD4$^+$ T-cell counts after SIVmac239 challenge. (A) Relative CD4$^+$ T-cell counts after challenge in A$^+$ (upper left), E$^+$ (upper right), B$^+$ (lower left), and J$^+$ (lower right) macaques. For each animal, the peripheral CD4 counts relative to that at challenge (set at 100) are shown. (B) Changes in means of relative CD4$^+$ T-cell counts after challenge in A$^+$ (black), E$^+$ (blue), B$^+$ (green), and J$^+$ (red) animals. (C) Comparison of relative CD4$^+$ T-cell counts at 6 months among four groups. Those in J$^+$ animals were significantly lower than those in A$^+$ ($P = 0.0090$ by one-way ANOVA and Tukey-Kramer's multiple-comparison test).

differences in set point plasma viral loads between groups A$^+$ and J$^+$ (Fig. 1C).

Most noncontrollers showed a decline in peripheral CD4$^+$ T-cell counts (Fig. 2A). Relative CD4$^+$ T-cell counts in the chronic phase were the highest in group A$^+$ animals and the lowest in group J$^+$ animals. Multiple-comparison tests revealed significant differences in relative CD4$^+$ T-cell counts at 6 months between groups A$^+$ and J$^+$ (Fig. 2B and C). Furthermore, multiple comparisons among groups A$^+$, E$^+$, and J$^+$ found significant differences in survival periods, which were the longest in A$^+$ and the shortest in J$^+$ animals (Table 2 and Fig. 3). These results indicate an association of MHC-I haplotypes with AIDS progression after SIV challenge in Burmese rhesus macaques.

**SIV antigen-specific CD8$^+$ T-cell responses.** We analyzed SIV-specific CD8$^+$ T-cell responses at 3 months and 1 year after SIV challenge by the detection of antigen-specific IFN-γ induction to examine which antigen-specific CD8$^+$ T-cell responses were induced predominantly (Table 3). Analysis revealed the predominant induction of Gag-specific and Nef-specific CD8$^+$ T-cell responses in group A$^+$ animals and Nef-specific CD8$^+$ T-cell responses in groups E$^+$ and B$^+$. Vif-specific CD8$^+$ T-cell responses were detected in three J$^+$ animals but not macaque R06-022, which rapidly developed AIDS in 5 months without detectable SIV-specific CD8$^+$ T-cell responses.

There was no significant difference in whole SIV antigen-specific CD8$^+$ T-cell responses among these four groups, although those responses were marginal or undetectable in two of four J$^+$ animals (Fig. 4A). However, Gag-specific CD8$^+$ T-cell frequencies at 3 months were significantly higher in A$^+$ animals (Fig. 4B). The analysis of four groups revealed inverse correlations between Gag-specific CD8$^+$ T-cell frequencies and plasma viral loads at 3 months ($P = 0.0087$; $r^2 = 0.3407$; data not shown). Three groups of A$^+$, E$^+$, and B$^+$ animals tended to show higher Nef-specific CD8$^+$ T-cell responses than J$^+$ animals (Fig. 4C).

**Viral genome mutations.** We then analyzed mutations in viral cDNAs amplified from plasma RNAs of group A$^+$, E$^+$, and B$^+$

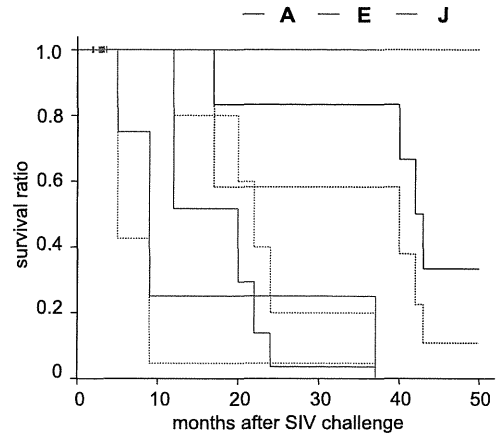


FIG 3 Kaplan-Meyer survival curves after SIVmac239 challenge in $A^+$, $E^+$, and $J^+$ macaques. Macaque R08-003, which is under observation, is not included. $B^+$ animals were excluded from this analysis because data on only two animals were available. We determined the Kaplan-Meyer estimate of the survival function of each group and then compared the three curves using the log-rank test (Mantel-Cox test). Analysis showed significant differences in survival curves (chi square, 9.9; $P = 0.007$ by log-rank test of Kaplan-Meyer estimates).

macaques around 1 year after SIV challenge. Nonsynonymous mutations detected predominantly were as shown in Fig. 5. Multiple comparisons among groups $A^+$, $E^+$, and $B^+$ (Fig. 6) showed no differences in total numbers of nonsynonymous mutations but revealed significantly higher numbers of *gag* mutations in $A^+$ animals. $E^+$ animals had higher numbers of *tat* mutations than $A^+$ animals. There was no significant difference in the numbers of mutations in other regions, including *nef*, among these groups. Group $J^+$ animals were not included in the multiple comparisons, because three of them were euthanized by 9 months. These three had lower numbers of nonsynonymous mutations before their death, possibly reflecting lower immune pressure.

**Polyfunctionality in SIV-specific T-cell responses.** Finally, we investigated T-cell polyfunctionality to compare T-cell functions (2, 4, 45) in these four groups having different viral loads. We analyzed the polyfunctionality of SIV-specific $CD4^+$ and $CD8^+$ T cells around 8 months after challenge by the detection of SIV-specific induction of IFN-γ, TNF-α, IL-2, MIP-1β, and CD107a. SIV-specific $CD4^+$ T-cell polyfunctionality inversely correlated with plasma viral loads at around 9 months (Fig. 7A). We also found an inverse correlation between SIV-specific $CD8^+$ T-cell polyfunctionality and viral loads (Fig. 7A). However, there was no

TABLE 3 SIV antigen-specific $CD8^+$ T-cell responses[a]

| MHC-I haplotype and time point after challenge | Macaque | $CD8^+$ T-cell response to: | | | | | | | | |
|---|---|---|---|---|---|---|---|---|---|---|
| | | Gag | Pol | Vif | Vpx | Vpr | Tat | Rev | Env | Nef |
| 3 mo | | | | | | | | | | |
| A | R02-007 | ND | ND | ND | ND | ND | ND | ND | ND | ND |
| A | R06-037 | 657 | — | 104 | — | — | — | — | — | 520 |
| A | R07-001 | 193 | — | — | — | — | — | — | — | 322 |
| A | R07-004 | 316 | — | 137 | — | — | — | — | — | 353 |
| A | R07-009 | 440 | — | 124 | — | — | — | — | 100 | 247 |
| A | R06-019 | 322 | — | — | — | — | — | — | — | 253 |
| E | R01-011 | — | — | 186 | — | — | — | — | — | — |
| E | R05-007 | — | — | — | — | — | 203 | — | — | 330 |
| E | R08-003 | — | — | — | — | — | — | — | — | 213 |
| E | R08-007 | — | — | — | — | — | — | — | 335 | — |
| E | R09-011 | — | — | 807 | — | 307 | — | — | 1,598 | 2,327 |
| E | R06-038 | 199 | — | 248 | — | — | 249 | — | 234 | 634 |
| B | R06-001 | — | 107 | 253 | 172 | — | — | — | 114 | 313 |
| B | R06-039 | — | — | — | — | — | — | — | 110 | 195 |
| B | R10-005 | 163 | 172 | — | 1,033 | 141 | — | 579 | — | 1,554 |
| B | R10-008 | — | — | — | 133 | — | — | 165 | — | — |
| J | R02-004 | — | — | 171 | — | — | 145 | — | 382 | 117 |
| J | R04-014 | — | 534 | 625 | 280 | 440 | 290 | 1,060 | — | 296 |
| J | R06-022 | — | — | — | — | — | — | — | — | — |
| J | R10-001 | — | — | 102 | — | — | — | — | — | — |
| 1 yr | | | | | | | | | | |
| A | R02-007 | — | — | 119 | — | — | — | — | 112 | 250 |
| A | R06-037 | 515 | — | 124 | 272 | 178 | — | — | — | 906 |
| A | R07-001 | 126 | — | — | — | — | — | — | — | 180 |
| A | R07-004 | — | — | — | — | — | — | — | — | 150 |
| A | R07-009 | 254 | 120 | 173 | — | 112 | — | — | 215 | 166 |
| A | R06-019 | 444 | 155 | 284 | — | 188 | — | — | 174 | 583 |
| E | R01-011 | 160 | — | — | — | — | — | — | — | 228 |
| E | R05-007 | — | — | — | — | — | — | — | — | — |
| E | R08-003 | — | — | — | — | — | — | — | — | 537 |
| E | R08-007 | — | — | — | — | — | — | — | — | 199 |
| E | R09-011 | — | 159 | — | — | — | — | 150 | 259 | 102 |
| E | R06-038 | 298 | 174 | 611 | — | — | 406 | 387 | 1,052 | 1,982 |
| B | R06-001 | — | — | — | — | — | — | — | 127 | 140 |
| B | R06-039 | — | — | — | — | — | 151 | — | — | — |
| B | R10-005 | 185 | — | — | — | — | — | — | — | — |
| B | R10-008 | 109 | 232 | — | — | — | — | 325 | — | 296 |
| J | R02-004 | 158 | — | — | — | — | — | — | — | — |
| J | R04-014[b] | 114 | 141 | 178 | — | — | 360 | 288 | — | 142 |
| J | R10-001[b] | — | — | — | — | — | — | — | — | — |

[a] Responses were measured by the detection of antigen-specific IFN-γ induction. Macaque R06-022, euthanized at 5 months, is not included in the lower portion. Antigen-specific $CD8^+$ T-cell frequencies (per 1 million PBMCs) are shown. ND, not determined; —, undetectable (<100).

[b] At 9 months (before euthanasia).

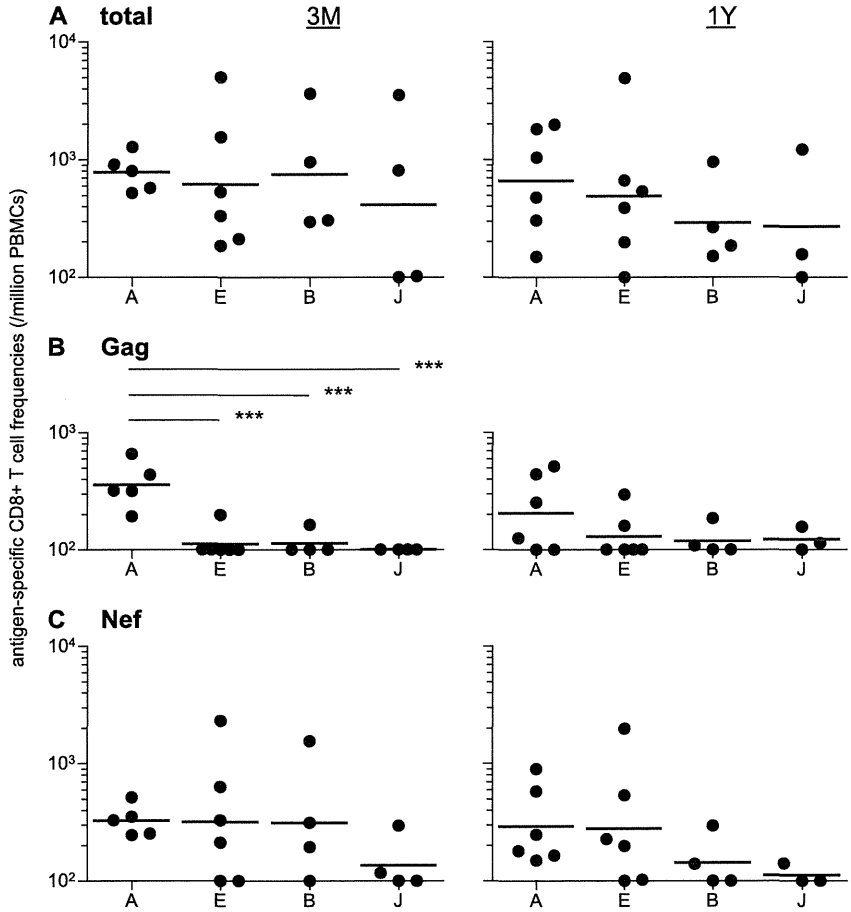


FIG 4 Comparison of SIV antigen-specific $CD8^+$ T-cell responses. Responses were measured by the detection of antigen-specific IFN-γ induction using PBMCs at 3 months (3 M; left) and at 1 year (1Y; right). (A) Whole SIV antigen-specific $CD8^+$ T-cell frequencies. The sum of Gag-, Pol-, Vif-, Vpx-, Vpr-, Tat-, Rev-, Env-, and Nef-specific $CD8^+$ T-cell frequencies in each animal is shown. (B) Gag-specific $CD8^+$ T-cell frequencies. The frequencies at 3 months in $A^+$ animals were significantly higher ($A^+$ and $E^+$, $P < 0.0001$; $A^+$ and $B^+$, $P = 0.0003$; $A^+$ and $J^+$, $P < 0.0001$ by one-way ANOVA and Tukey-Kramer's multiple-comparison test). (C) Nef-specific $CD8^+$ T-cell frequencies.

correlation between viral loads and total SIV-specific $CD4^+$ T-cell or $CD8^+$ T-cell frequencies (Fig. 7B). Polyfunctional T-cell responses tended to be higher in group $A^+$ and lower in group $J^+$. Multiple comparisons revealed significant differences in SIV-specific $CD4^+$ T-cell polyfunctionality with the highest in group $A^+$ and the lowest in group $J^+$ (Fig. 7C). These results may reflect difference in disease progression among these animals.

## DISCUSSION

This study describes SIVmac239 infection in 20 Burmese rhesus macaques. Geometric means of set point plasma viral loads were approximately $10^5$ copies/ml. The levels are considered lower than those usually observed in the widely used SIVmac239 infection model of Indian rhesus macaques (28, 55) but are higher than those typically observed in untreated humans infected with HIV-1. While two $A^+$ animals controlled SIV replication, the remaining 18 Burmese rhesus macaques failed to control viremia. Indeed, all of the animals in the three groups $E^+$, $B^+$, and $J^+$ showed persistent viremia. Those noncontrollers, including four $A^+$ animals, developed AIDS in 0.5 to 4 years. These results indicate that the SIVmac239 infection of Burmese rhesus macaques does serve as an AIDS model.

In the present study, we compared SIVmac239 infections among four groups sharing MHC-I haplotypes A, E, B, and J, respectively. These animals showed differences in plasma viral loads, peripheral $CD4^+$ T-cell counts, survival periods, patterns of viral antigen-specific $CD8^+$ T-cell responses, polyfunctionality of SIV-specific T-cell responses, and numbers of viral genome mutations. These results indicate the association of MHC-I haplotypes with AIDS progression. There has been a number of reports describing SIV infections in macaques sharing a single or a couple of MHC-I alleles, but few studies have examined SIV infection in macaques sharing an MHC-I haplotype (10, 11, 40). SIV infection induces multiple epitope-specific $CD8^+$ T-cell responses, and $CD8^+$ T-cell responses specific for some MHC-I-restricted epitopes can be affected by those specific for other MHC-I-restricted epitopes due to CTL immunodominance (16, 29, 52). Thus, the preparation of macaque groups sharing MHC-I genotypes at the haplotype level, as described in the present study, would contribute to the precise analysis of SIV infection. The establishment of groups sharing both MHC-I haplotypes (56) may be ideal, but the accumulation of macaque groups sharing even one MHC-I haplotype could lead to the constitution of a more sophisticated primate AIDS model.

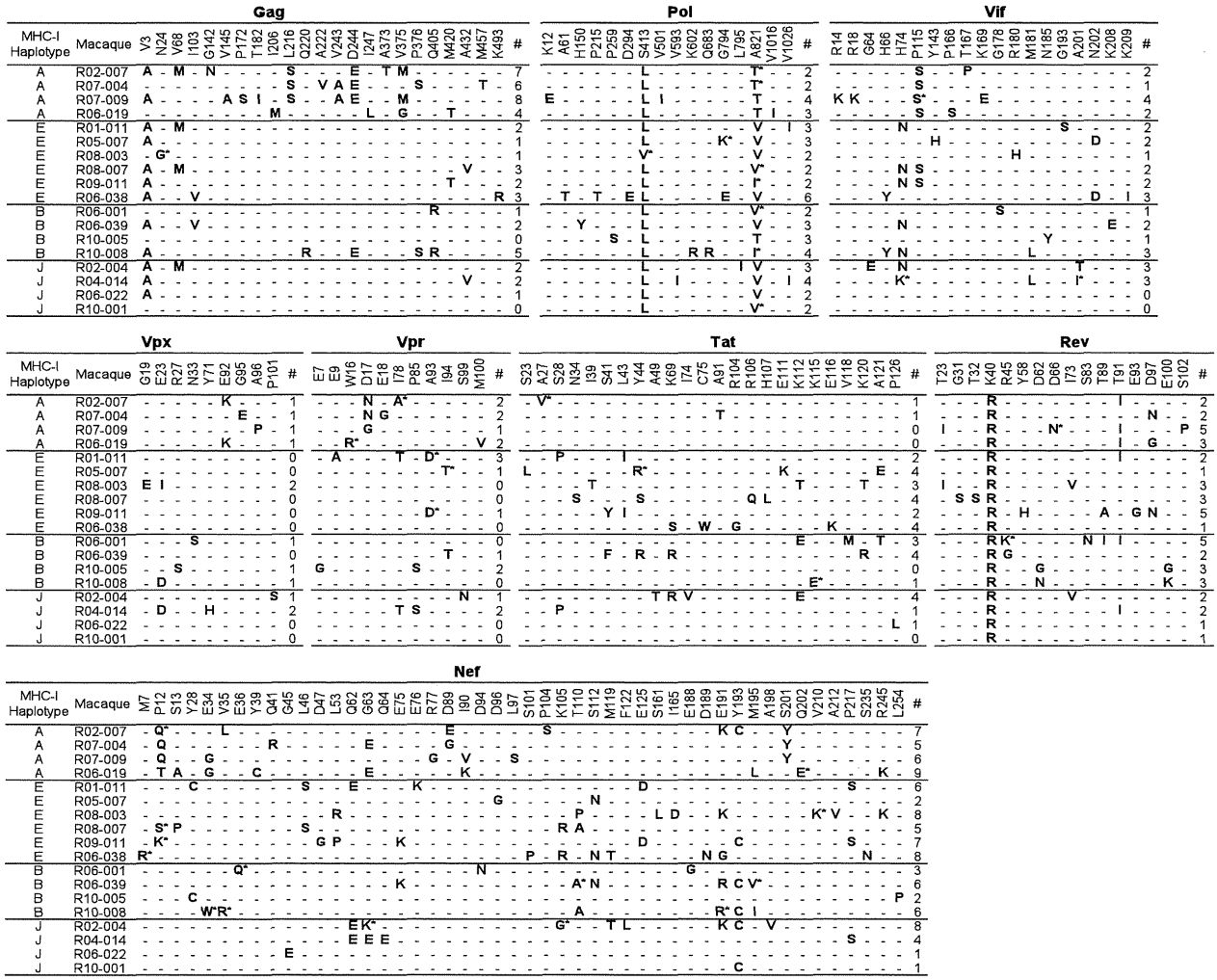


FIG 5 Predominant nonsynonymous mutations in viral cDNAs around 1 year after SIVmac239 challenge. Amino acid substitutions in SIV Gag, Pol, Vif, Vpx, Vpr, Tat, Rev, and Nef are shown. In three animals, R04-014, R06-022, and R10-001 in group $J^+$, data on the samples obtained before their death at 5 or 9 months after challenge are shown. Asterisks indicate the residues where different mutations were detected. It is known that amino acid substitutions at the Pol residues 413 and 821 and the Rev residue 40 are frequently observed in SIVmac239 infection and contribute to higher viral fitness *in vivo* (1, 39).

Various MHC-I alleles that do not consist of the first MHC-I haplotypes (A in $A^+$, E in $E^+$, B in $B^+$, and J in $J^+$ animals) were detected as shown in Table 4. Two $A^+$ macaques, R02-007 and R07-004, had two major alleles, *Mamu-A1*008:01* and *Mamu-B*007:02*, of MHC-I haplotype J, although their second MHC-I haplotype was not determined as J on the basis of information on the family tree. Even when these two animals were excluded from the $A^+$ group, multiple-comparison analyses showed significant

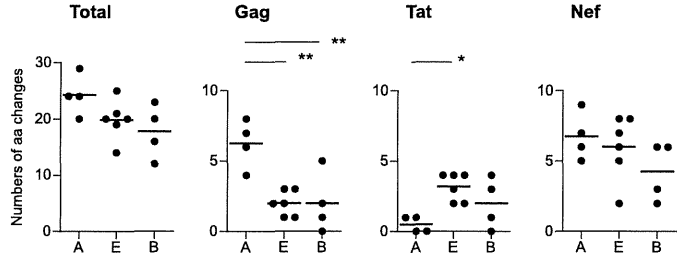


FIG 6 Comparison of the numbers of predominant nonsynonymous mutations in viral cDNAs around 1 year after SIVmac239 challenge among $A^+$, $E^+$, and $B^+$ macaques. $J^+$ animals were excluded from this analysis because three of them were euthanized by 1 year. The first graph (total) shows the sum of the numbers of amino acid substitutions in SIV Gag, Pol, Vif, Vpx, Vpr, Tat, Rev, and Nef. Gag, Tat, and Nef graphs show the numbers of Gag, Tat, and Nef amino acid substitutions, respectively. The numbers of Gag amino acid substitutions in $A^+$ animals were significantly higher than those in $E^+$ and $B^+$ animals ($A^+$ and $E^+$, $P = 0.0037$; $A^+$ and $B^+$, $P = 0.0069$ by one-way ANOVA and Tukey-Kramer's multiple-comparison test). The numbers of Tat amino acid substitutions in $E^+$ animals were significantly higher than those in $A^+$ animals ($P = 0.0140$).

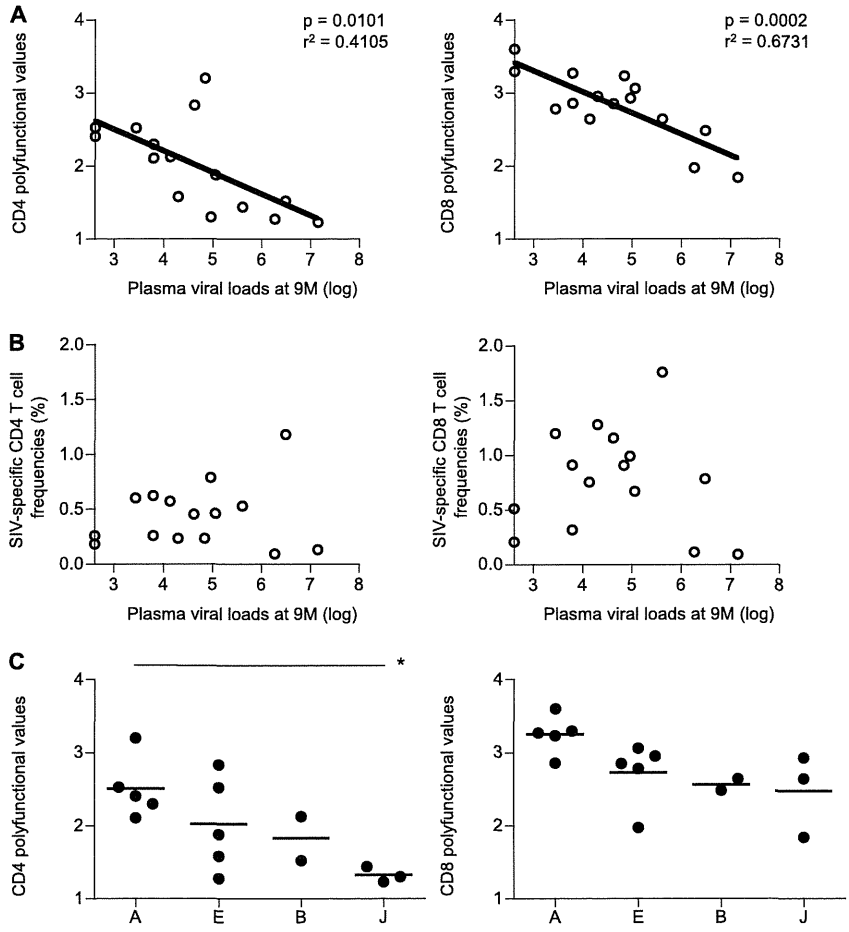


FIG 7 Polyfunctionality in SIV-specific $CD4^+$ and $CD8^+$ T cells around 8 months after SIVmac239 challenge. Samples of macaques R02-007 ($A^+$), R01-011 ($E^+$), R10-005 ($B^+$), R10-008 ($B^+$), and R10-001 ($J^+$) were unavailable. (A) Correlation analysis of plasma viral loads at 9 months with polyfunctionality (polyfunctional values) of SIV-specific $CD4^+$ (left) and $CD8^+$ (right) T cells. Viral loads inversely correlated with SIV-specific $CD4^+$ ($P = 0.0101$; $r^2 = 0.4105$) and $CD8^+$ ($P = 0.0002$; $r^2 = 0.6731$) T-cell polyfunctionality. (B) Correlation analysis of plasma viral loads at 9 months with SIV-specific $CD4^+$ (left) and $CD8^+$ (right) T-cell frequencies (frequencies of $CD4^+$ and $CD8^+$ T cells showing the SIV-specific induction of induction of IFN-γ, TNF-α, IL-2, MIP-1β, or CD107a). (C) SIV-specific $CD4^+$ (left) and $CD8^+$ (right) T-cell polyfunctionality in $A^+$ ($n = 5$), $E^+$ ($n = 5$), $B^+$ ($n = 2$), and $J^+$ ($n = 3$) macaques. Multiple comparisons among $A^+$, $E^+$, and $J^+$ animals (excluding the $B^+$ group with available data on only two animals) revealed significant difference in SIV-specific $CD4^+$ T-cell polyfunctionality ($A^+$ and $J^+$, $P = 0.0195$ by one-way ANOVA and Tukey-Kramer's multiple-comparison test).

differences in plasma viral loads, peripheral $CD4^+$ T-cell counts, survival periods, Gag-specific $CD8^+$ T-cell responses, and numbers of viral gag mutations. These two $A^+$ animals were noncontrollers, supporting the notion that CTL responses specific for Mamu-A1*008:01- or Mamu-B*007:02-restricted epitopes are not efficient or effective. In addition, several MHC-I alleles were shared in two or three animals, but the influence of these alleles on disease progression remains unclear.

In the group $A^+$ animals that showed lower viral loads and slower disease progression, Gag-specific $CD8^+$ T-cell responses were efficiently induced, and their frequencies were significantly higher than those in the other three groups. Furthermore, these $A^+$ animals had higher numbers of nonsynonymous *gag* mutations, possibly reflecting strong selective pressure by Gag-specific $CD8^+$ T-cell responses. Previously, $CD8^+$ T-cell responses specific for the $Gag_{206\text{-}216}$ (IINEEAADWDL) epitope restricted by MHC-I haplotype A-derived Mamu-A1*043:01 and the $Gag_{241\text{-}249}$ (SSVDEQIQW) epitope restricted by A-derived Mamu-A1*065:01 have been shown to exert strong suppressive pressure on SIV replication (19, 21). In the present study, most $A^+$ animals selected escape mutations from these $CD8^+$ T-cell responses, GagL216S (a mutation leading to a leucine [L]-to-serine [S] substitution at the 216th amino acid in Gag) and GagD244E (aspartic acid [D]-to-glutamic acid [E] substitution at the 244th amino acid) or I247L (isoleucine [I]-to-L substitution at the 247th amino acid). These results are consistent with recent findings suggesting the potential of Gag-specific $CD8^+$ T-cell responses to efficiently suppress HIV-1/SIV replication (24).

In SIV-infected $A^+$ animals, predominantly Nef-specific as well as Gag-specific $CD8^+$ T-cell responses were elicited. At 3 months postchallenge, all of the $A^+$ animals showed relatively similar levels of total antigen-specific, Gag-specific, and Nef-specific $CD8^+$ T-cell responses, and their deviations appeared to be less than those in the other three groups. This may reflect the diminished influence of the second MHC-I haplotypes in these $A^+$ animals in the early phase of SIV infection, i.e., $CD8^+$ T-cell responses specific for epitopes restricted by MHC-I molecules derived from the second haplotypes may be suppressed by dominant $CD8^+$ T-cell responses specific for A-derived MHC-I-restricted epitopes.

TABLE 4 Alleles in the second MHC-I haplotypes in macaques[a]

| Group | Macaque | Allele(s) |
|---|---|---|
| $A^+$ | R02-007 | *A1*008:01, B*007:02* |
| $A^+$ | R06-037 | *A1*052:01, A2*005:13, B*089:02/03*[b] |
| $A^+$ | R07-001 | *A1*032:02, B*066:01* |
| $A^+$ | R07-004 | *A1*008:01, B*007:02, B*039:01* |
| $A^+$ | R07-009 | ND[c] |
| $A^+$ | R06-019 | *A1*032:02, A2*005:02, B*106:01, B*124:01* |
| $E^+$ | R01-011 | *A1*004:01, B*004:01, B*060:03, B*102:01* |
| $E^+$ | R05-007 | *A1*032:03, B*042:01, B*066:01, B*089:01* |
| $E^+$ | R08-003 | *B*074:02, B*101:01* |
| $E^+$ | R08-007 | *A2*005:10, B*054:02, B*061:04, B*063:02, B*124:01* |
| $E^+$ | R09-011 | *A1*041:02, B*061:02, B*068:04/05*[d] |
| $E^+$ | R06-038 | *A1*004:01, A-new,*[e] *B*001:01, B*007:02/03, B*017:03* |
| $B^+$ | R06-001 | *A1*008:01* |
| $B^+$ | R06-039 | *A1*032:02, B*004:01, B*033:01, B*066:01, B*102:01* |
| $B^+$ | R10-005 | *A1*003:01, B*019:01* |
| $B^+$ | R10-008 | *B*026:02, B*045:07, B*051:06* |
| $J^+$ | R02-004 | ND[f] |
| $J^+$ | R04-014 | *A4*014:03, B*071:01* |
| $J^+$ | R06-022 | *A5*030:06, B*102:01* |
| $J^+$ | R10-001 | *A1*004:01, B*026:02, B*043:01, B*073:01* |

[a] Detected alleles not included in the first MHC-I haplotypes (A in $A^+$, E in $E^+$, B in $B^+$, or J in $J^+$ animals) are shown.
[b] The *Mamu-B* allele has sequences identical to *B*089:02* and *B*089:03* in exons 2 and 3.
[c] MHC-I alleles other than those consisting of the MHC-I haplotype A were not detected.
[d] The *Mamu-B* allele has sequences identical to *B*068:04* and *B*068:05* in exons 2 and 3.
[e] New *Mamu-A* allele 96% similar to *A1*018:03* by sequence homology in exons 2 and 3.
[f] MHC-I alleles other than those consisting of the MHC-I haplotype J were not detected.

Nef-specific $CD8^+$ T-cell responses were induced efficiently at 3 months or 1 year postchallenge in groups $A^+$, $E^+$, and $B^+$ but not in most $J^+$ animals, which showed higher viral loads and rapid disease progression. The former three groups had relatively higher numbers of nonsynonymous *nef* mutations, which correlated with Nef-specific $CD8^+$ T-cell responses at 1 year ($P = 0.0063$; $r^2 = 0.4765$; data not shown). Thus, these Nef-specific $CD8^+$ T-cell responses, whose suppressive pressure might be less than that of Gag-specific ones, may play roles in the suppression of SIV replication, while we have not determined Nef epitopes for those $CD8^+$ T-cell responses exerting strong suppressive pressure. No nef mutations common to each group were detected, which suggests multiple Nef epitope-specific $CD8^+$ T-cell responses. Regarding the Nef-specific $CD8^+$ T-cell responses in SIV-infected $E^+$ animals, some Nef epitopes are speculated to be restricted by E-derived MHC-I molecules. Our results, however, indicate that primary SIV infection induces no predominant $CD8^+$ T-cell responses specific for Gag epitopes restricted by E-derived MHC-I molecules in the early phase. In $J^+$ animals, we found no predominant $CD8^+$ T-cell responses specific for J-derived, MHC-I-restricted epitopes in the early phase of SIV infection.

This study indicates differences in the patterns of CTL immunodominance among these groups. Gag-specific $CD8^+$ T-cell responses were induced in group $A^+$, showing slower disease progression, and Nef-specific CTL responses were induced in those animals other than group $J^+$ animals, which showed rapid disease progression. These results can be reasonably explained by the differences in MHC-I haplotypes, although it is difficult to completely rule out the possibility of disease progression associating with other genes located around the MHC-I locus. In our previous study (21), the challenge of $A^+$ macaques with a mutant SIVmac239 carrying GagL216S and GagD244E mutations showed higher set point viral loads, indicating that these A-derived, MHC-I-restricted, $Gag_{206\text{-}216}$ and $Gag_{241\text{-}249}$ epitope-specific $CD8^+$ T-cell responses are responsible for lower viral loads in group $A^+$ animals.

Our analysis revealed differences in the target antigens for predominant $CD8^+$ T-cell responses but not in the magnitudes of SIV-specific $CD8^+$ T-cell responses among four groups. However, we found differences in polyfunctional SIV-specific $CD4^+$ T-cell responses in the chronic phase. Remarkably, plasma viral loads inversely correlated with the polyfunctionality of SIV-specific $CD8^+$ T cells as well as $CD4^+$ T cells. These results suggest stronger polyfunctional T cell responses in animals with lower viral loads, which, conversely, could contribute to the sustained suppression of viral replication in the chronic phase.

In summary, we examined SIVmac239 infection in four groups of Burmese rhesus macaques, with each group sharing different MHC-I haplotypes. Our results indicate the association of MHC-I haplotypes with disease progression. This study presents a robust AIDS model of SIV infection facilitating the analysis of virus-host immune interaction.

## ACKNOWLEDGMENTS

This work was supported by grants-in-aid from the Ministry of Education, Culture, Sports, Science, and Technology, grants-in-aid from the Ministry of Health, Labor, and Welfare, and a grant from Takeda Science Foundation in Japan.

The animal experiments were conducted through the Cooperative Research Program in Tsukuba Primate Research Center, National Institute of Biomedical Innovation, with the help of the Corporation for Production and Research of Laboratory Primates.

We thank F. Ono, K. Oto, A. Hiyaoka, K. Komatsuzaki, M. Hamano, Y. Emoto, H. Akari, and Y. Yasutomi for their assistance in animal experiments. We also thank M. Roederer for providing the PESTLE and SPICE software.

## REFERENCES

1. **Alexander L, Denekamp L, Czajak S, Desrosiers RC.** 2001. Suboptimal nucleotides in the infectious, pathogenic simian immunodeficiency virus clone SIVmac239. J. Virol. **75**:4019–4022.
2. **Almeida JR, et al.** 2007. Superior control of HIV-1 replication by CD8+ T cells is reflected by their avidity, polyfunctionality, and clonal turnover. J. Exp. Med. **204**:2473–2485.
3. **Altfeld M, et al.** 2003. Influence of HLA-B57 on clinical presentation and viral control during acute HIV-1 infection. AIDS **17**:2581–2591.
4. **Betts MR, et al.** 2006. HIV nonprogressors preferentially maintain highly functional HIV-specific CD8+ T cells. Blood **107**:4781–4789.
5. **Bontrop RE, Watkins DI.** 2005. MHC polymorphism: AIDS susceptibility in non-human primates. Trends Immunol. **26**:227–233.
6. **Borrow P, Lewicki H, Hahn BH, Shaw GM, Oldstone MB.** 1994. Virus-specific CD8+ cytotoxic T-lymphocyte activity associated with control of viremia in primary human immunodeficiency virus type 1 infection. J. Virol. **68**:6103–6110.
7. **Boyson JE, et al.** 1996. The MHC class I genes of the rhesus monkey. Different evolutionary histories of MHC class I and II genes in primates. J. Immunol. **156**:4656–4665.
8. **Carrington M, et al.** 1999. HLA and HIV-1: heterozygote advantage and B*35-Cw*04 disadvantage. Science **283**:1748–1752.
9. **Daza-Vamenta R, Glusman G, Rowen L, Guthrie B, Geraghty DE.** 2004.

Genetic divergence of the rhesus macaque major histocompatibility complex. Genome Res. 14:1501–1515.
10. **Evans DT, et al.** 1999. Virus-specific cytotoxic T-lymphocyte responses select for amino-acid variation in simian immunodeficiency virus Env and Nef. Nat. Med. 5:1270–1276.
11. **Evans DT, et al.** 2000. Definition of five new simian immunodeficiency virus cytotoxic T-lymphocyte epitopes and their restricting major histocompatibility complex class I molecules: evidence for an influence on disease progression. J. Virol. 74:7400–7410.
12. **Feinberg MB, Moore JP.** 2002. AIDS vaccine models: challenging challenge viruses. Nat. Med. 8:207–210.
13. **Goulder PJ, Watkins DI.** 2004. HIV and SIV CTL escape: implications for vaccine design. Nat. Rev. Immunol. 4:630–640.
14. **Goulder PJ, Watkins DI.** 2008. Impact of MHC class I diversity on immune control of immunodeficiency virus replication. Nat. Rev. Immunol. 8:619–630.
15. **Guidotti LG, Chisari FV.** 2000. Cytokine-mediated control of viral infections. Virology 273:221–227.
16. **Ishii H, et al.** 2012. Impact of vaccination on cytotoxic T lymphocyte immunodominance and cooperation against simian immunodeficiency virus replication in rhesus macaques. J. Virol. 86:738–745.
17. **Iwamoto N, et al.** 2010. Broadening of CD8+ cell responses in vaccine-based simian immunodeficiency virus controllers. AIDS 24:2777–2787.
18. **Jin X, et al.** 1999. Dramatic rise in plasma viremia after CD8(+) T cell depletion in simian immunodeficiency virus-infected macaques. J. Exp. Med. 189:991–998.
19. **Kawada M, et al.** 2006. Involvement of multiple epitope-specific cytotoxic T-lymphocyte responses in vaccine-based control of simian immunodeficiency virus replication in rhesus macaques. J. Virol. 80:1949–1958.
20. **Kawada M, et al.** 2007. Long-term control of simian immunodeficiency virus replication with central memory CD4+ T-cell preservation after nonsterile protection by a cytotoxic T-lymphocyte-based vaccine. J. Virol. 81:5202–5211.
21. **Kawada M, et al.** 2008. Gag-specific cytotoxic T-lymphocyte-based control of primary simian immunodeficiency virus replication in a vaccine trial. J. Virol. 82:10199–10206.
22. **Kestler HW, III, et al.** 1991. Importance of the nef gene for maintenance of high virus loads and for development of AIDS. Cell 65:651–662.
23. **Kiepiela P, et al.** 2004. Dominant influence of HLA-B in mediating the potential co-evolution of HIV and HLA. Nature 432:769–775.
24. **Kiepiela P, et al.** 2007. CD8+ T-cell responses to different HIV proteins have discordant associations with viral load. Nat. Med. 13:46–53.
25. **Koup RA, et al.** 1994. Temporal association of cellular immune responses with the initial control of viremia in primary human immunodeficiency virus type 1 syndrome. J. Virol. 68:4650–4655.
26. **Kulski JK, Anzai T, Shiina T, Inoko H.** 2004. Rhesus macaque class I duplicon structures, organization and evolution within the alpha block of the major histocompatibility complex. Mol. Biol. Evol. 21:2079–2091.
27. **Leslie A, et al.** 2010. Additive contribution of HLA class I alleles in the immune control of HIV-1 infection. J. Virol. 84:9879–9888.
28. **Letvin NL, et al.** 2006. Preserved CD4+ central memory T cells and survival in vaccinated SIV-challenged monkeys. Science 312:1530–1533.
29. **Loffredo JT, et al.** 2008. Patterns of CD8+ immunodominance may influence the ability of Mamu-B*08-positive macaques to naturally control simian immunodeficiency virus SIVmac239 replication. J. Virol. 82: 1723–1738.
30. **Loffredo JT, et al.** 2007. Mamu-B*08-positive macaques control simian immunodeficiency virus replication. J. Virol. 81:8827–8832.
31. **Matano T, et al.** 2004. Cytotoxic T lymphocyte-based control of simian immunodeficiency virus replication in a preclinical AIDS vaccine trial. J. Exp. Med. 199:1709–1718.
32. **Matano T, et al.** 1998. Administration of an anti-CD8 monoclonal antibody interferes with the clearance of chimeric simian/human immunodeficiency virus during primary infections of rhesus macaques. J. Virol. 72: 164–169.
33. **Migueles SA, et al.** 2000. HLA B*5701 is highly associated with restriction of virus replication in a subgroup of HIV-infected long term nonprogressors. Proc. Natl. Acad. Sci. U. S. A. 97:2709–2714.
34. **Miura T, et al.** 2009. HLA-B57/B*5801 human immunodeficiency virus type 1 elite controllers select for rare gag variants associated with reduced viral replication capacity and strong cytotoxic T-lymphocyte recognition. J. Virol. 83:2743–2755.
35. **Morgan C, et al.** 2008. The use of nonhuman primate models in HIV vaccine development. PLoS Med. 5:e173.
36. **Mothe BR, et al.** 2003. Expression of the major histocompatibility complex class I molecule Mamu-A*01 is associated with control of simian immunodeficiency virus SIVmac239 replication. J. Virol. 77:2736–2740.
37. **Muhl T, Krawczak M, Ten Haaft P, Hunsmann G, Sauermann U.** 2002. MHC class I alleles influence set-point viral load and survival time in simian immunodeficiency virus-infected rhesus monkeys. J. Immunol. 169:3438–3446.
38. **Naruse TK, et al.** 2010. Diversity of MHC class I genes in Burmese-origin rhesus macaques. Immunogenetics 62:601–611.
39. **O'Connor DH, et al.** 2002. Acute phase cytotoxic T lymphocyte escape is a hallmark of simian immunodeficiency virus infection. Nat. Med. 8:493–499.
40. **O'Connor SL, et al.** 2010. MHC heterozygote advantage in simian immunodeficiency virus-infected Mauritian cynomolgus macaques. Sci. Transl. Med. 2:22ra18.
41. **Otting N, et al.** 2005. Unparalleled complexity of the MHC class I region in rhesus macaques. Proc. Natl. Acad. Sci. U. S. A. 102:1626–1631.
42. **Roederer M, Nozzi JL, Nason MC.** 2011. SPICE: exploration and analysis of post-cytometric complex multivariate datasets. Cytometry A 79:167–174.
43. **Schmitz JE, et al.** 1999. Control of viremia in simian immunodeficiency virus infection by CD8+ lymphocytes. Science 283:857–860.
44. **Seder RA, Hill AV.** 2000. Vaccines against intracellular infections requiring cellular immunity. Nature 406:793–798.
45. **Seder RA, Darrah PA, Roederer M.** 2008. T-cell quality in memory and protection: implications for vaccine design. Nat. Rev. Immunol. 8:247–258.
46. **Shibata R, et al.** 1997. Infection and pathogenicity of chimeric simian-human immunodeficiency viruses in macaques: determinants of high virus loads and CD4 cell killing. J. Infect. Dis. 176:362–373.
47. **Sodora DL, et al.** 2009. Toward an AIDS vaccine: lessons from natural simian immunodeficiency virus infections of African nonhuman primate hosts. Nat. Med. 15:861–865.
48. **Stinchcombe JC, Bossi G, Booth S, Griffiths GM.** 2001. The immunological synapse of CTL contains a secretory domain and membrane bridges. Immunity 15:751–761.
49. **Takahara Y, et al.** 2011. Dominant induction of vaccine antigen-specific cytotoxic T lymphocyte responses after simian immunodeficiency virus challenge. Biochem. Biophys. Res. Commun. 408:615–619.
50. **Tanaka-Takahashi Y, et al.** 2007. Reference strand-mediated conformation analysis-based typing of multiple alleles in the rhesus macaque MHC class I Mamu-A and Mamu-B loci. Electrophoresis 28:918–924.
51. **Tang J, et al.** 2002. Favorable and unfavorable HLA class I alleles and haplotypes in Zambians predominantly infected with clade C human immunodeficiency virus type 1. J. Virol. 76:8276–8284.
52. **Tenzer S, et al.** 2009. Antigen processing influences HIV-specific cytotoxic T lymphocyte immunodominance. Nat. Immunol. 10:636–646.
53. **Tsukamoto T, et al.** 2009. Impact of cytotoxic-T-lymphocyte memory induction without virus-specific CD4+ T-cell help on control of a simian immunodeficiency virus challenge in rhesus macaques. J. Virol. 83:9339–9346.
54. **Wang YE, et al.** 2009. Protective HLA class I alleles that restrict acute-phase CD8+ T-cell responses are associated with viral escape mutations located in highly conserved regions of human immunodeficiency virus type 1. J. Virol. 83:1845–1855.
55. **Wilson NA, et al.** 2006. Vaccine-induced cellular immune responses reduce plasma viral concentrations after repeated low-dose challenge with pathogenic simian immunodeficiency virus SIVmac239. J. Virol. 80:5875–5885.
56. **Wiseman RW, et al.** 2007. Simian immunodeficiency virus SIVmac239 infection of major histocompatibility complex-identical cynomolgus macaques from Mauritius. J. Virol. 81:349–361.
57. **Yamamoto H, Kawada M, Takeda A, Igarashi H, Matano T.** 2007. Post-infection immunodeficiency virus control by neutralizing antibodies. PLoS One 2:e540.
58. **Yamamoto T, et al.** 2009. Polyfunctional CD4+ T-cell induction in neutralizing antibody-triggered control of simian immunodeficiency virus infection. J. Virol. 83:5514–5524.
59. **Yant LJ, et al.** 2006. The high-frequency major histocompatibility complex class I allele Mamu-B*17 is associated with control of simian immunodeficiency virus SIVmac239 replication. J. Virol. 80:5074–5077.

Leukemia (2012), 1–4

www.nature.com/leu

LETTER TO THE EDITOR

# Direct binding of Grb2 has an important role in the development of myeloproliferative disease induced by ETV6/FLT3

*Leukemia* advance online publication, 14 December 2012; doi:10.1038/leu.2012.333

FMS-like tyrosine kinase 3 (*FLT3*) is one of the most frequently mutated genes in hematological malignancies.[1] The most common mutations of *FLT3* are internal tandem duplications (ITDs) within the juxtamembrane domain, which occur in 20% to 30% of patients with acute myeloid leukemia (AML).[2,3] Although FLT3 is a potential therapeutic target in AML, recent studies involving FLT3 inhibitors as single agents in patients with AML showed limited clinical responses.[4] FLT3 has been reported to fuse to ETV6 (TEL) in a few cases of myeloid/lymphoid neoplasms with eosinophilia (MLN-eo) carrying a translocation t(12;13)(p13;q12).[5,6] Although it has been shown that ETV6/FLT3 acts as a constitutively active tyrosine kinase, the molecular mechanisms underlying ETV6/FLT3-mediated leukemogenesis remain incompletely understood.[7–9]

We identified a novel *ETV6/FLT3* variant fusion transcript (E/F-1) in a MLN-eo patient (Supplementary Figures S1A and B) and investigated the transforming properties of ETV6/FLT3 *in vivo* using a murine bone marrow transplant (BMT) model.[10,11] E/F-1-transduced recipients developed an aggressive polyclonal myeloproliferative disease (MPD) in 100% of recipient mice with a latency of 3-4 weeks, as evidenced by marked leukocytosis, splenomegaly and massive expansion of myeloid cells in peripheral blood, spleen and bone marrow (Figures 1A–C). In this mice model, eosinophilia was not observed. Flow cytometric analysis of the peripheral blood from E/F-1 mice showed a large population of EGFP$^+$/Mac-1$^+$/Gr-1$^+$ cells. In primary E/F-1 mice, serial passage was performed by transferring a 1:1 mixture of spleen and bone marrow cells to sublethally irradiated recipient mice. This resulted in hematopoietic malignancies in most of the recipient mice receiving five different primary tumors. For three of the primary tumors, it was possible to transmit the MPD for at least one round. In all cases of serial passage, the MPD transformed into aggressive T-lymphoblastic lymphoma (T-LBL) with a latency of 4–17 weeks (Figure 1E, Supplementary Figure S2B). Most lymphoma occurred in the thymus or abdominal lymph nodes, and some of the secondary recipient mice displayed leukocytosis, generalized lymphadenopathy or hepatosplenomegaly. Histopathological examination revealed that the architecture of the lymph nodes and the thymus was completely effaced and that they contained a uniform population of lymphoblasts. The liver showed prominent periportal, lobular and sinusoidal infiltration by lymphoma cells (Figure 1D). Flow cytometric analysis of spleen cells revealed that the lymphomas typically showed an immature T-cell immunophenotype characterized by expression of both CD4 and CD8 (Supplementary Figure S2A). Affected tissues from secondary diseased mice contained proviral integrations identical to those in the primary MPD mouse (Figure 1F). ETV6/FLT3-induced T-LBL was transplantable, with all tertiary transplant recipients rapidly succumbing to T-LBL at 4–7 weeks after transfer arising from common clones identified in the secondary mice (Supplementary Figure S2C).

Previous studies have shown that FLT3-ITDs induce a lethal MPD in mice and that tyrosine residues 589 and 591 in the juxtamembrane domain of FLT3 are critical for STAT5 phosphorylation and generation of the MPD phenotype.[10] We also demonstrated the corresponding results for FLT3-ITD in our murine BMT experiment (Supplementary Figures S3A and B). On the other hand, mice that received the double tyrosine-to-phenylalanine mutant of E/F-1 at sites 589 and 591 (Y589/591F) in the juxtamembrane domain of FLT3 developed a similar MPD (Supplementary Table S1). There was no significant difference in survival between recipients of E/F-1 vs Y589/591F, with both mice groups succumbing to a fatal MPD within a median survival time of 18 and 19.5 days, respectively ($P = 0.284$; Figure 1C). The Y589/591F mutation did not abrogate STAT5, Erk1/2 and Akt activation in Ba/F3 cells transformed by E/F-1 (Supplementary Figure S4), which is consistent with the previous studies using a deletion mutant of the FLT3 juxtamembrane domain in ETV6/FLT3.[9]

Growth factor receptor-binding protein 2 (Grb2) is an adaptor protein known to bind several receptor tyrosine kinases. Grb2 binds the scaffolding protein Grb2-associated binder 2 (Gab2) and contributes to survival signaling in ligand-activated wild-type FLT3.[12] A recent study has shown that tyrosines 768, 955 and 969 of FLT3 are the direct Grb2-binding sites of importance for FLT3-ITD-mediated proliferation and survival of hematopoietic cells *in vitro* as a result of STAT5 activation via Gab2.[13] However, there have been no reports regarding the *in vivo* effects of direct Grb2 binding by oncogenic FLT3 in leukemogenesis. Thus, we investigated the role of Grb2 binding in ETV6/FLT3-mediated leukemogenesis. Inspection of the ETV6 portion of the fusion protein revealed only two candidate tyrosines for direct binding of Grb2 at positions 314 and 354. To test whether Grb2 binds directly to ETV6/FLT3, we made a series of Grb2-binding mutants of ETV6/FLT3 (Figure 2a). The Y314/354F double point mutant (2F) and the Y768/955/969F triple mutant (3F-1) of E/F-1 showed a reduced ability to bind Grb2 as compared with the E/F-1. Furthermore, when we mutated tyrosines 314 or 354 to phenylalanine in the context of the Y768/955/969F triple mutant, the association of ETV6/FLT3 with Grb2 was significantly reduced as compared with the Y768/955/969F triple mutant. Finally, when we mutated all five specific tyrosines (Y314/354/768/955/969) to phenylalanine, we observed that ETV6/FLT3 was no longer able to bind Grb2 (Figure 2b). Simultaneous mutation of these five tyrosine residues resulted in an absence of Gab2 phosphorylation, and impaired activation of STAT5, Erk1/2 and Akt in Ba/F3 cells (Figure 2c). ETV6/FLT3 variant E/F-2, which lacked the Grb2-binding sites of ETV6, was unable to bind to Grb2 when all three Grb2-binding sites of FLT3 were mutated (Figure 2b). This Y768/955/969F triple mutant of E/F-2 (3F-2) was also unable to phosphorylate Gab2 and showed weaker activation of STAT5, Erk1/2 and Akt as compared with E/F-2 in Ba/F3 cells (Figure 2c). Both E/F-1 and E/F-2 transformed bone marrow cells to be capable of cytokine-independent growth in methylcellulose medium. Transformation was significantly decreased in the 5F and 3F-2 mutants, which

Accepted article preview online 20 November 2012

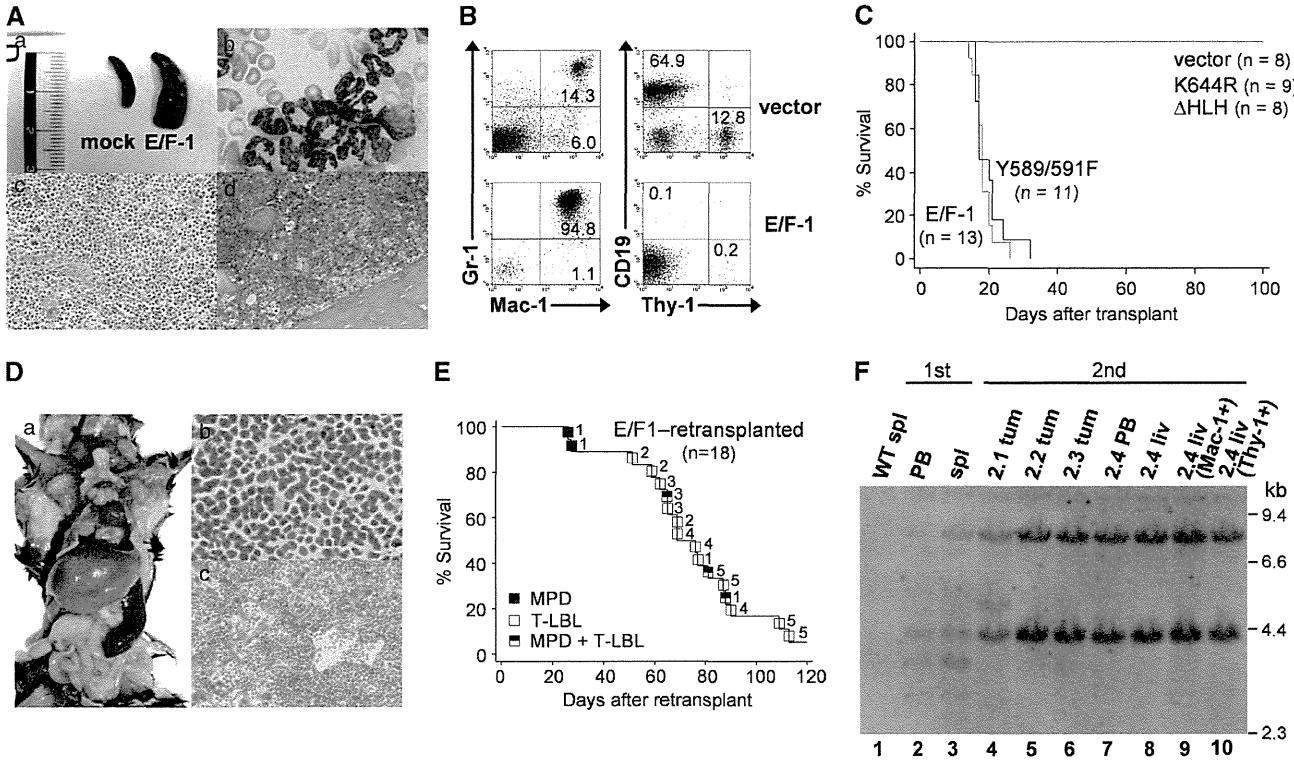


**Figure 1.** ETV6/FLT3 induces a rapidly fatal MPD in primary recipient mice, which transformed into T-LBL and MPD during serial passage. (**A**) (a) Splenomegaly associated with MPD. (b) Representative May–Giemsa-stained peripheral blood smear of the diseased mouse ( × 100). (c, d) Representative hematoxylin and eosin-stained bone marrow (c) and spleen (d) of the diseased mouse ( × 20). (**B**) Flow cytometric analysis of cells from the peripheral blood of vector control and E/F-1 mice. The percentages of cells in quadrants of interest are shown. (**C**) Survival curve for recipients of bone marrow transduced with a vector control ($n = 8$), E/F-1 ($n = 13$), Y589/591F mutant ($n = 11$), kinase-inactive K644R mutant ($n = 9$) or deletion mutant of the HLH oligomerization domain of ETV6 (ΔHLH) ($n = 8$). Mice transplanted with a vector control, K644R, or ΔHLH remain free of disease 180 days after transplant. Survival data are cumulative from two or three separate experiments for all retroviral constructs. (**D**) (a) Macroscopic examination of a secondary recipient with T-LBL (b and c) Hematoxylin and eosin-stained lymph node (b) and liver (c) of the diseased mouse ( × 100 and × 20, respectively). (**E**) Kaplan–Meier survival analysis of the secondary recipients. Most secondary recipients succumbed to T-LBL or/and MPD. Pairs of recipients transplanted with cells from the same primary donor are indicated by numbers. (**F**) Proviral integrations in cells isolated from primary and secondary recipients. Genomic DNA isolated from the indicated tissues of a wild-type (WT) mouse (lane 1), a primary MPD mouse (lanes 2 and 3) and four secondary T-LBL mice receiving bone marrow and spleen from the same primary MPD mouse (lanes 4–10) was digested with *Eco*RI and analyzed for proviral integrations by hybridization with a DIG-labeled EGFP probe. Lanes 4–6 are DNAs from the tumors of mice with T-LBL. Lanes 7–10 represent lineage analysis from a single secondary mouse, which developed both MPD and T-LBL (2.4). The peripheral blood of the 2.4 mouse contained 83.5% EGFP$^+$Mac-1$^+$ and 10.6% EGFP$^+$Thy-1$^+$ cells, and the liver of the 2.4 mouse contained 27.2% EGFP$^+$Mac-1$^+$ and 58.8% EGFP$^+$Thy-1$^+$ cells at the time of euthanization. The MACS-sorted liver myeloid (Mac-1$^+$) and T cells (Thy-1$^+$) from this mouse were 98.1% and 98.4% pure, respectively. DNA size markers (in kb) are shown on the right. liv, liver; PB, peripheral blood; spl, spleen; tum, tumor.

were unable to bind Grb2, but not in 2F and 3F-1 mutants (Figure 2d). To examine the contribution of Grb2 binding to ETV6/FLT3-induced MPD *in vivo*, we performed BMT experiments. White blood cell (WBC) counts and spleen weights of the mice receiving 5F-transduced bone marrow were significantly lower than those receiving E/F-1-transduced bone marrow (Supplementary Table S1). Flow cytometric analyses of spleen cells showed that 5F mice had a reduced fraction of Mac-1$^+$/Gr-1$^+$ cells compared with E/F-1 mice (Supplementary Figure S5A). 5F mice showed significantly less infiltrate in the hepatic lobules or periportal areas than the E/F-1 mice (Supplementary Figure S5B). Recipients of both 2F and 3F-1 developed rapidly fatal MPD with a comparable latency to those of E/F-1. Survival of 5F and 3F-2 mice was significantly prolonged compared with that of E/F-1 and E/F-2 mice, respectively (55 days vs 18 days, 73 days vs 13 days, respectively; $P < 0.001$; Figure 2e), although most 5F and 3F-2 recipient mice eventually succumbed to MPD.

Finally, we compared the ability of ETV6/FLT3 to transform primary myeloid cells from the bone marrow of Gab2$^{-/-}$ and Gab2$^{+/+}$ mice. Expression of E/F-1 in Gab2$^{-/-}$ cells resulted in an approximately threefold lower number of cytokine-independent CFU-C (Supplementary Figure S6A). We assessed the relative contribution of the *Gab2* gene to ETV6/FLT3-mediated leukemogenesis in BMT experiments using Gab2$^{-/-}$ and Gab2$^{+/+}$ donor mice. All mice transplanted with Gab2$^{+/+}$ bone marrow cells expressing ETV6/FLT3 developed severe MPD (median WBC, $236 \times 10^3/\mu l$; spleen weight, 561 mg), as expected (Supplementary Figure S6B). ETV6/FLT3-induced myeloproliferation was attenuated in mice transplanted with Gab2$^{-/-}$ bone marrow cells expressing ETV6/FLT3 (median WBC, $31 \times 10^3/\mu l$; spleen weight, 350 mg). Survival of mice injected with Gab2$^{-/-}$ bone marrow cells expressing E/F-1 was significantly prolonged in comparison with those injected with Gab2$^{+/+}$ cells (56 days vs 21 days, $P < 0.001$; Figure 2f), although all recipients of Gab2$^{-/-}$ background bone marrow cells eventually succumbed to MPD.

Our results suggest that ETV6/FLT3 has more potent oncogenic activity than FLT3-ITDs and can transform progenitor cells with the capacity to differentiate into myeloid and lymphoid progeny, supporting the contention that human *ETV6/FLT3*-positive MLN-eo is a stem cell disorder. Unlike FLT3-ITDs, mice that received the

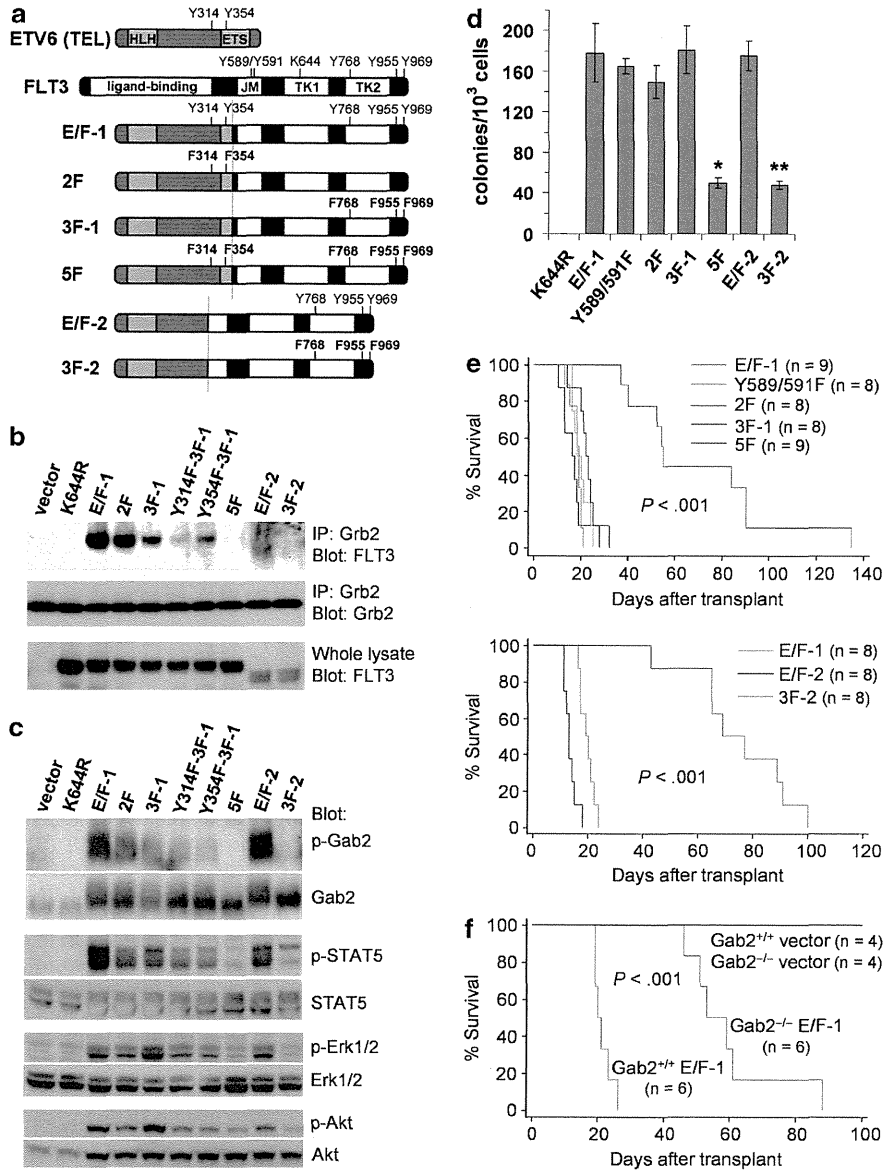


**Figure 2.** Both ETV6 and FLT3 portions contribute to ETV6/FLT3-mediated leukemogenesis via Grb2-Gab2 pathway. (**a**) Schematic representation of ETV6/FLT3 fusion proteins including the series of Grb2-binding site mutants. The point of fusion is indicated by a vertical dotted line. E/F-1 was cloned by us. E/F-2 was cloned previously (Vu *et al.*[5]). (**b**) Coimmunoprecipitation: lysates from Ba/F3 cells expressing the indicated ETV6/FLT3 proteins were immunoprecipitated using an anti-Grb2 antibody and blotted with anti-FLT3 (top) and anti-Grb2 (middle) antibodies. Whole-cell lysates were also blotted with the anti-FLT3 antibody (bottom). As a control, lysates from vector-transduced cells were included. Three independent experiments were performed and representative data are shown. (**c**) Activation of downstream targets was demonstrated by blotting the whole-cell lysates of Ba/F3 cells with the indicated phosphospecific antibodies. After stripping, the membranes were reprobed with the indicated total antibodies. Three independent experiments were performed and representative data are shown. (**d**) Cytokine-independent colony formation of whole bone marrow cells expressing ETV6/FLT3 wild-type or Grb2-binding mutants. The difference between E/F-1 and 5F (*) and between E/F-2 and 3F-2 (**) is statistically significant ($P<0.001$, unpaired *t*-test). Data are the mean ± s.d. of three independent experiments. (**e**) Survival curve for recipients of bone marrow transduced with ETV6/FLT3 and Grb2-binding mutants. Both E/F-1 and E/F-2 mice caused rapidly fatal MPD. 5F mutant mice and 3F-2 mutant mice developed MPD with a longer median survival of 55 and 73 days, respectively ($P<0.001$ vs E/F-1 and E/F-2, respectively). One of the 5F mutant mice died of severe anemia without showing any signs of MPD. Survival data are cumulative from two or three separate experiments for all retroviral constructs. (**f**) Survival curve for recipients of Gab2$^{-/-}$ and Gab2$^{+/+}$ bone marrow transduced with a vector control or E/F-1. The *P*-value represents a comparison of survival by E/F-1 on Gab2$^{-/-}$ vs Gab2$^{+/+}$ background.

Y589/591F mutant of ETV6/FLT3 also developed a lethal MPD with a short latency. The reason for the discrepancy between ETV6/FLT3 and FLT3-ITDs is not clear. This may be due to altered structural conformation of ETV6/FLT3 relative to wild-type FLT3 or alternatively, it may be due to different subcellular localization of the fusion protein and FLT3-ITDs.[14,15] Recently it was reported that sunitinib and sorafenib, tyrosine kinase inhibitors with multiple targets including FLT3, had therapeutic efficacy in two patients with *ETV6/FLT3*-positive MLN-eo.[6] Unfortunately, similar to most of the patients with *FLT3-ITD*-positive AML, relapse and resistance occurred in both patients. Although clinical application of Grb2 inhibitors remains limited to just a phase I trial of a liposomal antisense for hematological malignancies, the results of the current study indicate therapeutic potential against Grb2 in

patients with *ETV6/FLT3*-positive MLN-eo. In addition, previous studies have shown that the Grb2-Gab2 pathway also has an important role in FLT3-ITD-mediated cell proliferation and survival.[13,15] These findings suggest that inhibition of this pathway may be useful in the treatment of FLT3-associated leukemia.

## CONFLICT OF INTEREST

The authors declare no conflict of interest.

## ACKNOWLEDGEMENTS

This work was supported in part by grants from the Ministry of Education, Culture, Sports, Science and Technology of Japan (MH).

K Chonabayashi[1], M Hishizawa[1], S Kawamata[2], Y Nagai[1], T Ohno[3], T Ishikawa[1], T Uchiyama[1] and A Takaori-Kondo[1]
*[1]Department of Hematology and Oncology, Graduate School of Medicine, Kyoto University, Kyoto, Japan;*
*[2]Foundation for Biomedical Research and Innovation, Kobe, Japan and*
*[3]Division of Hematology and Immunology, Department of Internal Medicine, Ohtsu Red Cross Hospital, Ohtsu, Japan*
*E-mail: hishiza@kuhp.kyoto-u.ac.jp*

## REFERENCES

1 Stirewalt DL, Radich JP. The role of FLT3 in haematopoietic malignancies. *Nat Rev Cancer* 2003; **3**: 650–665.
2 Kiyoi H, Naoe T, Nakano Y, Yokota S, Minami S, Miyawaki S *et al.* Prognostic implication of FLT3 and N-RAS gene mutations in acute myeloid leukemia. *Blood* 1999; **93**: 3074–3080.
3 Thiede C, Steudel C, Mohr B, Schaich M, Schakel U, Platzbecker U *et al.* Analysis of FLT3-activating mutations in 979 patients with acute myelogenous leukemia: association with FAB subtypes and identification of subgroups with poor prognosis. *Blood* 2002; **99**: 4326–4335.
4 Kindler T, Lipka DB, Fischer T. FLT3 as a therapeutic target in AML: still challenging after all these years. *Blood* 2010; **116**: 5089–5102.
5 Vu HA, Xinh PT, Masuda M, Motoji T, Toyoda A, Sakaki Y *et al.* FLT3 is fused to ETV6 in a myeloproliferative disorder with hypereosinophilia and a t(12;13)(p13;q12) translocation. *Leukemia* 2006; **20**: 1414–1421.
6 Walz C, Erben P, Ritter M, Bloor A, Metzgeroth G, Telford N *et al.* Response of ETV6-FLT3-positive myeloid/lymphoid neoplasm with eosinophilia to inhibitors of FMS-like tyrosine kinase 3. *Blood* 2011; **118**: 2239–2242.
7 Tse KF, Mukherjee G, Small D. Constitutive activation of FLT3 stimulates multiple intracellular signal transducers and results in transformation. *Leukemia* 2000; **14**: 1766–1776.
8 Baldwin BR, Li L, Tse KF, Small S, Collector M, Whartenby KA *et al.* Transgenic mice expressing Tel-FLT3, a constitutively activated form of FLT3, develop myeloproliferative disease. *Leukemia* 2007; **21**: 764–771.
9 Vu HA, Xinh PT, Kano Y, Tokunaga K, Sato Y. The juxtamembrane domain in ETV6/FLT3 is critical for PIM-1 up-regulation and cell proliferation. *Biochem Biophys Res Commun* 2009; **383**: 308–313.
10 Rocnik JL, Okabe R, Yu JC, Lee BH, Giese N, Schenkein DP *et al.* Roles of tyrosine 589 and 591 in STAT5 activation and transformation mediated by FLT3-ITD. *Blood* 2006; **108**: 1339–1345.
11 Tanaka Y, Era T, Nishikawa S, Kawamata S. Forced expression of Nanog in hematopoietic stem cells results in a gammadeltaT-cell disorder. *Blood* 2007; **110**: 107–115.
12 Zhang S, Broxmeyer HE. Flt3 ligand induces tyrosine phosphorylation of gab1 and gab2 and their association with shp-2, grb2, and PI3 kinase. *Biochem Biophys Res Commun* 2000; **277**: 195–199.
13 Masson K, Liu T, Khan R, Sun J, Ronnstrand L. A role of Gab2 association in Flt3 ITD mediated Stat5 phosphorylation and cell survival. *Br J Haematol* 2009; **146**: 193–202.
14 Schmidt-Arras DE, Bohmer A, Markova B, Choudhary C, Serve H, Bohmer FD. Tyrosine phosphorylation regulates maturation of receptor tyrosine kinases. *Mol Cell Biol* 2005; **25**: 3690–3703.
15 Choudhary C, Olsen JV, Brandts C, Cox J, Reddy PN, Bohmer FD *et al.* Mislocalized activation of oncogenic RTKs switches downstream signaling outcomes. *Mol Cell* 2009; **36**: 326–339.

Supplementary Information accompanies this paper on the Leukemia website (http://www.nature.com/leu)

# Human CD1c$^+$ Myeloid Dendritic Cells Acquire a High Level of Retinoic Acid–Producing Capacity in Response to Vitamin $D_3$

Takayuki Sato,*,† Toshio Kitawaki,* Haruyuki Fujita,* Makoto Iwata,†,‡ Tomonori Iyoda,†,§ Kayo Inaba,†,§ Toshiaki Ohteki,†,¶ Suguru Hasegawa,‖ Kenji Kawada,‖ Yoshiharu Sakai,‖ Hiroki Ikeuchi,# Hiroshi Nakase,** Akira Niwa,††,‡‡ Akifumi Takaori-Kondo,* and Norimitsu Kadowaki*,†

**All-*trans*-retinoic acid (RA) plays a critical role in maintaining immune homeostasis. Mouse intestinal CD103$^+$ dendritic cells (DCs) produce a high level of RA by highly expressing retinal dehydrogenase (RALDH)2, an enzyme that converts retinal to RA, and induce gut-homing T cells. However, it has not been identified which subset of human DCs produce a high level of RA. In this study, we show that CD1c$^+$ blood myeloid DCs (mDCs) but not CD141$^{high}$ mDCs or plasmacytoid DCs exhibited a high level of RALDH2 mRNA and aldehyde dehydrogenase (ALDH) activity in an RA- and p38-dependent manner when stimulated with 1α,25-dihydroxyvitamin $D_3$ ($VD_3$) in the presence of GM-CSF. The ALDH activity was abrogated by TLR ligands or TNF. CD103$^-$ rather than CD103$^+$ human mesenteric lymph node mDCs gained ALDH activity in response to $VD_3$. Furthermore, unlike in humans, mouse conventional DCs in the spleen and mesenteric lymph nodes gained ALDH activity in response to GM-CSF alone. RALDH2$^{high}$ CD1c$^+$ mDCs stimulated naive CD4$^+$ T cells to express gut-homing molecules and to produce Th2 cytokines in an RA-dependent manner. This study suggests that CD1c$^+$ mDCs are a major human DC subset that produces RA in response to $VD_3$ in the steady state. The "vitamin D – CD1c$^+$ mDC – RA" axis may constitute an important immune component for maintaining tissue homeostasis in humans.** *The Journal of Immunology*, **2013, 191: 3152–3160.**

Dendritic cells (DCs) play a pivotal role in controlling immune responses in terms of their magnitude and quality, such as immunity versus tolerance, depending on the tissue milieu. This eventually leads to maintaining immune homeostasis by eliminating pathogens and by avoiding harmful inflammation. Recent studies using mice revealed the importance of all-*trans*-retinoic acid (hereafter referred to as RA) derived from DCs in maintaining immune homeostasis in the intestine (1) and possibly in other organs (2). It has been shown that CD103$^+$ DCs in lamina propria and mesenteric lymph nodes (MLNs) produce RA and thus to promote the generation of gut-homing regulatory T (Treg) cells (3). GM-CSF (4) and RA (4–8) are pivotal factors to induce mouse DCs to express retinal dehydrogenase (RALDH)2, which is encoded by the aldehyde dehydrogenase 1 family, member A2 (*ALDH1A2*) gene and converts retinal to RA. IL-4 (4, 9) and TLR ligands (2, 4, 5, 10–12) augment the expression of RALDH2. These studies have presented a model that appropriately stimulated CD103$^+$ DCs in gut-associated tissues produce RA and thus induce gut-homing Treg cells, resulting in maintaining immune homeostasis in the intestine in mice. Surprisingly, however, human DCs that express a high level of RALDH have not been identified.

Human DC subsets in blood and lymphoid tissues are composed of myeloid DCs (mDCs) and plasmacytoid DCs (pDCs) (13). mDCs are further subdivided into CD141 (BDCA-3)$^{high}$ mDCs and CD1c (BDCA-1)$^+$ mDCs, and the former corresponds to mouse CD8$^+$ CD11b$^-$ conventional DCs (cDCs) in lymphoid tissues (14–16) and CD103$^+$ cDCs in nonlymphoid tissues (17) that efficiently cross-present Ags. In contrast, distinctive functions of the latter, which is likely equivalent to mouse CD8$^-$CD11b$^+$ cDCs (18), have been elusive. In addition, monocytes and CD34$^+$ hematopoietic progenitors can differentiate into DCs in the presence of appropriate cytokine mixtures. However, it remains unclear which DCs in situ correspond to DCs induced in vitro from monocytes or CD34$^+$ progenitors. Therefore, it is important to obtain data using DCs isolated from blood and tissues to gain an insight into physiological and clinical relevance of basic researches on human DCs.

*Department of Hematology and Oncology, Graduate School of Medicine, Kyoto University, Kyoto 606-8507, Japan; †Japan Science and Technology Agency, Core Research for Evolutional Science and Technology, Tokyo 102-0076, Japan; ‡Laboratory of Immunology, Kagawa School of Pharmaceutical Sciences, Tokushima Bunri University, Kagawa 769-2193, Japan; §Division of Systemic Life Science, Department of Animal Development and Physiology, Laboratory of Immunology, Graduate School of Biostudies, Kyoto University, Kyoto 606-8501, Japan; ¶Department of Biodefense Research, Medical Research Institute, Tokyo Medical and Dental University, Tokyo 101-0062, Japan; ‖Department of Surgery, Graduate School of Medicine, Kyoto University, Kyoto 606-8507, Japan; #Department of Surgery, Hyogo College of Medicine, Hyogo 663-8501, Japan; **Department of Gastroenterology and Hepatology, Graduate School of Medicine, Kyoto University, Kyoto 606-8507, Japan; ††Department of Pediatrics, Graduate School of Medicine, Kyoto University, Kyoto 606-8507, Japan; and ‡‡Department of Clinical Application, Center for iPS Cell Research and Application, Kyoto University, Kyoto 606-8507, Japan

Received for publication December 26, 2012. Accepted for publication July 16, 2013.

This work was supported by research funding from the Japan Science and Technology Agency, Core Research for Evolutional Science and Technology (to N.K.).

Address correspondence and reprint requests to Dr. Norimitsu Kadowaki, Department of Hematology and Oncology, Graduate School of Medicine, Kyoto University, 54 Shogoin Kawahara-cho, Sakyo-ku, Kyoto 606-8507, Japan. E-mail address: kadowaki@kuhp.kyoto-u.ac.jp

The online version of this article contains supplemental material.

Abbreviations used in this article: ALDH, aldehyde dehydrogenase; ALDH1A2, aldehyde dehydrogenase 1 family, member A2; cDC, conventional dendritic cell; CLA, cutaneous lymphocyte Ag; DC, dendritic cell; DEAB, diethylaminobenzaldehyde; GUSB, β-glucuronidase; mDC, myeloid DC; MFI, mean fluorescence intensity; MLN, mesenteric lymph node; MoDC, monocyte-derived DC; pDC, plasmacytoid DC; PE-Cy5, PE-Cyanin 5; RA, all-*trans*-retinoic acid; RALDH, retinal dehydrogenase; RAR, pan-RA receptor; rh, recombinant human; Treg, regulatory T; $VD_3$, 1α,25-dihydroxyvitamin $D_3$; VDR, vitamin D receptor.



www.jimmunol.org/cgi/doi/10.4049/jimmunol.1203517

In the current study, we used human DCs from blood and MLNs, as well as DCs induced from monocytes or $CD34^+$ progenitors in vitro, and explored 1) DC subsets that express a high level of RALDH2, 2) factors that induce human DCs to express a high level of RALDH2, 3) differences between humans and mice in RA-producing DC subsets and RA-inducing factors, 4) intracellular mechanisms by which RALDH2 is induced in DCs, and 5) T cell responses induced by RA-producing DCs in an RA-dependent manner. To quantify the activity of RALDH in mouse (2, 4, 5, 7, 8, 12, 19) and human (5, 19) DCs, recent studies used the Aldefluor reagent that freely diffuses into cells and is converted to a fluorescent product by aldehyde dehydrogenase (ALDH) activity. Thus, we used this reagent in combination with quantitation of ALDH1A2 mRNA to quantify the RA-producing capacity of DCs. We found that only $CD1c^+$ mDCs are capable of expressing a high level of RALDH2 in response to 1α,25-dihydroxyvitamin $D_3$ ($VD_3$) together with GM-CSF and that the $RALDH2^{high}$ mDCs induce T cells to preferentially express gut-homing molecules and Th2 cytokines in an RA-dependent manner. This study thus reveals a previously unrecognized distinctive function of human $CD1c^+$ mDCs and an unexpected role of vitamin D, that is, induction of RA from human DCs.

## Materials and Methods

### *Culture media*

RPMI 1640 (Nacalai tesque) supplemented with 10% heat-inactivated FCS (ThermoTrace), 2 mM L-glutamine, penicillin G, streptomycin (Life Technologies), and 10 mM HEPES were used for cell culture.

### *Reagents*

Reagents and sources were as follows: recombinant human (rh)TNF, rhIL-3, rh stem cell factor, rhFLT3 ligand (PeproTech); rhGM-CSF (sargramostim; Genzyme); R848 (InvivoGen); LPS (from *Escherichia coli* O111:B4; Sigma-Aldrich); $PGE_2$ (MP Biomedicals); rhIL-2 (teceleukin; Shionogi & Co.); recombinant mouse GM-CSF (Kirin Brewery); anti-human IL-4 (clone MP4-25D2; eBioscience); anti-human CD28 mAbs (BD Biosciences); LE540 (Wako); U0126 (Cayman Chemical); SB203580, SP600125 (InvivoGen); VX-745 (Tocris); JAK inhibitor I (pyridone 6; Calbiochem); and SB239063 (Enzo Life Sciences). The inhibitors were dissolved in DMSO. Immunomodulatory factors added to DCs are listed in Table I. The following reagents were used for ELISA: anti–human IFN-γ mAb (clone 2G1 as capture Ab), biotinylated anti–human IFN-γ mAb (as detection Ab) and HRP-conjugated streptavidin (Endogen), OptEIA human IL-4 and IL-10 ELISA set (BD Biosciences), human IL-5 ELISA MAX Standard set (BioLegend), and a human IL-13 CytoSets kit (BioSource International).

The following Abs were used to stain human cells and are denoted as "fluorochrome-Ag." FITC-CD45RO, CD14, CD16, CD20, $\beta_7$ integrin, and cutaneous lymphocyte Ag (CLA), Alexa Fluor 488-CD1c, PE-CD103, $\alpha_4$ integrin, and CD203c, PE-Cyanin 5 (PE-Cy5)-CD4, PE-Cyanin 7-CD4, and Brilliant Violet 421-CD1c were from BioLegend; FITC-CD3 and HLA-DR, PE-CD11c and CD25, and PE-Cy5-CD11c from BD Biosciences; allophycocyanin-CD141 from Miltenyi Biotec; allophycocyanin-CCR9 (clone 248621) were from R&D Systems.

The following Abs were used to stain mouse cells and are denoted as fluorochrome-Ag. FITC-B220, PE-CD11c, and allophycocyanin-CD8 were from BD Biosciences; allophycocyanin-CD103 were from BioLegend.

### *Cell preparations*

This study was approved by the Institutional Review Board at Graduate School of Medicine, Kyoto University, and abides by the tenets of the Declaration of Helsinki. All specimens from humans were obtained from healthy donors and patients with written informed consent. To isolate human blood DCs, total PBMCs were depleted of $CD3^+$, $CD14^+$, and $CD16^+$ cells using Dynabeads goat anti-mouse IgG (Invitrogen Dynal). Then, $CD4^+CD11c^+CD141^{-/low}lin^-$ cells ($CD1c^+$ mDCs), $CD4^+CD141^{high}lin^-$ cells ($CD141^{high}$ mDCs), and $CD4^+CD11c^-CD141^{-/low}lin^-$ cells (pDCs) were purified using FACSAria cell sorter (BD Biosciences) (Supplemental Fig. 1A). The expression of CD1c on sorted blood $CD1c^+$ mDCs, $CD141^{high}$ mDCs, and pDCs is shown in Supplemental Fig. 1B. More than 98% of sorted cells were HLA-DR positive (Supplemental Fig. 1C). $CD203c^+$ basophils were isolated by sorting. Naive $CD4^+$ T cells and resting Treg cells (20) were $CD4^{high}CD25^-CD45RO^-$ cells and $CD4^{high}CD25^+CD45RO^-$ cells, respectively. Reanalysis of the sorted cells confirmed a purity of >98%. $CD8^+$ T cells were isolated from PBMCs using CD8 MicroBeads (Miltenyi Biotec).

Human MLNs from patients with colon cancer or Crohn's disease were obtained at Kyoto University Hospital or Hyogo College of Medicine Hospital, respectively. Single-cell suspension of MLNs was obtained by digestion with 500 μg/ml collagenase IV (Wako) and DNase I (Sigma-Aldrich) for 30 min, followed by sorting $CD4^+CD11c^+CD103^+lin^-CD141^{low/int}$ ($CD103^+$ mDCs), $CD4^+CD11c^+CD103^-lin^-CD141^{low/int}$ ($CD103^-$ mDCs), and $CD4^+CD11c^-CD103^-lin^-CD141^{low/int}$ (pDCs) as sorting strategy for blood DCs (Supplemental Fig. 1D). More than 99% of sorted cells were HLA-DR positive (Supplemental Fig. 1E).

Mouse $CD8^+$ and $CD8^-$ splenic DCs were prepared from BALB/c mice as described previously (Supplemental Fig. 1F) (21).

Single-cell suspensions from BALB/c mouse MLNs were prepared by collagenase (Boehringer-Ingerheim) digestion. Low-density cells were separated with BSA gradient centrifugation (Sigma-Aldrich), stained with PE-conjugated anti-CD11c, FITC-conjugated anti-B220, and allophycocyanin-conjugated anti-CD103 mAbs. DCs were first positively enriched using anti-PE microbeads (Mitenyi Biotec), and then, $CD103^+CD11c^+B220^-$ cells and $CD103^-CD11c^+B220^-$ cells were isolated as $CD103^+$ cDCs and $CD103^-$ cDCs, respectively (Supplemental Fig. 1G).

### *Cell culture*

Human blood $CD1c^+$ mDCs, $CD141^{high}$ mDCs, and monocytes were cultured with 800 U/ml GM-CSF for 2 d. Blood pDCs were cultured with 10 ng/ml IL-3 for 2 d. Human mDCs and mouse cDCs from MLNs were cultured with 800 U/ml GM-CSF for 24 h. Human MLN pDCs were cultured with 10 ng/ml IL-3 for 24 h. Mouse splenic cDCs were cultured with 800 U/ml GM-CSF for 24 h. During these cultures, soluble factors (reagents in Table I, TLR ligands, TNF, $PGE_2$, LE540, or pharmacological inhibitors) were added as indicated. Concentrations of the reagents other than those listed on Table I were 10 μg/ml R848, 1 μg/ml LPS, 100 ng/ml $Pam_3CSK_4$, 10 ng/ml TNF, 1 μg/ml $PGE_2$, 1 μM LE540, 20 μM SB203580, 10 μM SP600125, and 20 μM U0126. LE540 and the pharmacological inhibitors were added to the cultures 30 min before adding other reagents. To quantify cell viability, the percentages of propidium iodide–negative cells were measured by flow cytometry after cell debris was excluded by appropriate forward scatter thresholds.

### *Generation of DCs from monocytes and $CD34^+$ progenitor cells*

Monocytes were purified from PBMCs using CD14 MicroBeads (Miltenyi Biotec) and cultured with 800 U/ml GM-CSF and 500 U/ml IL-4 for 7 d to induce immature monocyte-derived DCs (MoDCs). LPS (100 ng/ml) was added during the last 2 d to induce maturation. Immunomodulatory factors (Table I) were added during the whole culture periods. To generate umbilical cord blood $CD34^+$ progenitor cell–derived DCs, $CD34^+$ cells were isolated using CD34 MicroBeads (Miltenyi Biotec) from cord blood and were cultured with 20 ng/ml stem cell factor, 50 ng/ml FLT3 ligand, 800 U/ml GM-CSF, and 2.5 ng/ml TNF for 7 d. Then, the cells were cultured in the absence or presence of RA, $VD_3$, or LPS (1 μg/ml) for 2 d.

### *Aldefluor assays and analysis of surface molecules*

ALDH activity was determined using the Aldefluor staining kit (StemCell Technology) according to the manufacturer's protocol. Diethylaminobenzaldehyde (DEAB) (Wako) was used as an ALDH inhibitor. T cells cocultured with DCs were stained with mAbs for $\alpha_4$ integrin, $\beta_7$ integrin, CLA, or CCR9. Live cells gated as propidium iodide–negative cells were acquired by FACSCalibur (BD Biosciences). Data were analyzed with FlowJo (Tree Star).

### *Reverse transcription and real-time PCR*

$CD1c^+$ mDCs, $CD141^{high}$ mDCs, and pDCs were cultured with indicated stimuli for 24 h. Total RNA was isolated using Homogenizer and the PureLink RNA Micro Kit (Invitrogen). First-strand cDNA synthesis was performed with the ReverTra Ace qPCR RT Kit (Toyobo). Real-time PCR was performed on the Thermal Cycler Dice Real-Time System (TaKaRa). ALDH1A1, ALDH1A2, ALDH1A3, CYP27B1, vitamin D receptor (VDR), and β-glucronidase (GUSB) were detected using TaqMan Gene Expression Assays (Applied Biosystems) and THUNDERBIRD Probe qPCR Mix (Toyobo). Primer and probe sets were as follows: *ALDH1A1*, Hs00946916_m1; *ALDH1A2*, Hs00180254_m1; *ALDH1A3*, Hs00167476_m1; *CYP27B1*, Hs00168017_m1; *VDR*, Hs01045840_m1; and *GUSB*, Hs00930627_m1.

The mRNA expression levels of each gene were normalized to those of *GUSB*.

### *T cell cultures with DCs*

After extensive wash, $CD1c^+$ mDCs ($1 \times 10^4$ cells) cultured with GM-CSF, RA, or $VD_3$ for 2 d were cocultured with allogeneic naive $CD4^+$ T cells or total $CD8^+$ T cells ($1 \times 10^5$ cells) in the absence or presence of 1 μM LE540, 10 μg/ml rat IgG1, or 10 μg/ml anti–IL-4 mAb in 96-well U-bottom plates for 6 d. IL-2 (10 U/ml) was added to $CD8^+$ T cell culture. The $CD4^+$ T cells were restimulated at $1 \times 10^6$ cells/ml with plate-bound anti-CD3 (OKT3) and 1 μg/ml soluble anti-CD28 mAbs in 96-well flat-bottom plates for 24 h. The supernatants were analyzed for cytokines by ELISA.

### *Statistical analysis*

Data are presented as the mean ± SE. Statistical comparisons were performed using paired two-tailed *t* test. Difference with $p < 0.05$ was considered significant.

## Results

### *Human blood $CD1c^+$ mDCs, but not $CD141^{high}$ mDCs, express a high level of RALDH2 in response to GM-CSF and $VD_3$*

In search of human DCs that express a high level of RALDH enzymes, different subsets of blood DCs were treated with various factors that have been reported to modulate immunostimulatory activity of DCs (Table I), and ALDH activity was measured with Aldefluor (2, 4, 5, 7, 8, 12, 19). To keep mDCs alive, we added GM-CSF (22) to $CD1c^+$ mDCs. GM-CSF by itself induced little ALDH activity (Fig. 1A, 1B). Adding RA with GM-CSF only slightly induced the activity, whereas $VD_3$, which modulates immunostimulatory properties of human mDCs and MoDCs (23–25), together with GM-CSF strongly upregulated the ALDH activity in $CD1c^+$ mDCs. RA plus $VD_3$ further augmented it (Fig. 1A, 1B). RA and $VD_3$ without GM-CSF induced little ALDH activity (Fig. 1A), indicating that GM-CSF is necessary for the induction. Ligands for TLRs (R848, LPS, and $Pam_3CSK_4$) and TNF strongly suppressed the ALDH activity, but $PGE_2$, which has been reported to suppress the ALDH activity in mouse bone marrow DCs (19), did not (Fig. 1C). There were no substantial differences in cell viability between different culture conditions at the time of harvest (data not shown). None of the other immunomodulatory factors (Table I) upregulated the ALDH activity in combination with GM-CSF (Supplemental Fig. 2).

In contrast to $CD1c^+$ mDCs, $CD141^{high}$ mDCs (Fig. 1D), pDCs (Fig. 1E), and CD34-derived DCs (Fig. 1F) cultured with RA and $VD_3$ exhibited little ALDH activity. RA and $VD_3$ without or with LPS slightly induced ALDH activity in MoDCs but at far lower levels than that in $CD1c^+$ mDCs (Fig. 1G). Consistent with a previous observation that human basophils express RALDH2 in response to IL-3 (26), IL-3 alone induced ALDH activity in basophils, but there was no augmentation with RA and $VD_3$ (Fig. 1H). There were no substantial differences in cell viability between different culture conditions (data not shown). Again, none of the other factors (Table I) upregulated the ALDH activity in combination with GM-CSF ($CD141^{high}$ mDCs, MoDCs) or IL-3 (pDCs) (Supplemental Fig. 2).

Table I. Immunomodulatory factors added to DCs

| Name | Concentrations | Sources |
|---|---|---|
| RA | 10 nM | Wako |
| $VD_3$ | 10 nM | Wako |
| IFN-α | 1000 U/ml | Intron A, Schering-Plough |
| IL-4 | 500 U/ml | PeproTech |
| TGF-β | 10 ng/ml | PeproTech |
| Vasoactive intestinal peptide | 100 nM | LKT Laboratories |
| Rosiglitazone | 10 μM | Alexis Biochemicals |
| T0901317 | 1 μM | Cayman Chemicals |
| Rapamycin | 100 ng/ml | PeproTech |
| Tacrolimus | 100 ng/ml | Enzo Life Sciences |
| Cyclosporin A | 1000 ng/ml | Sigma-Aldrich |
| Dexamethasone | 1 μM | Sigma-Aldrich |

We also cultured monocytes with GM-CSF in the absence or presence of the immunomodulatory factors (Table I). RA plus $VD_3$ substantially induced ALDH activity, albeit to a lesser extent than that in $CD1c^+$ mDCs. None of the other factors substantially induced the activity (Supplemental Fig. 2).

We next examined whether the ALDH activity detected by Aldefluor correlates with the expression levels of mRNA for *ALDH1A2* (encoding RALDH2) in $CD1c^+$ mDCs, $CD141^{high}$ mDCs, and pDCs. Consistent with the results by Aldefluor analyses, GM-CSF alone induced little expression of ALDH1A2 mRNA in $CD1c^+$ mDCs, and the addition of $VD_3$ markedly upregulated it (Fig. 1I). The addition of RA to GM-CSF and to GM-CSF plus $VD_3$ slightly increased the expression of ALDH1A2 mRNA, but R848 completely suppressed it. There was almost no expression of ALDH1A2 mRNA in $CD141^{high}$ mDCs or pDCs. mRNAs for *ALDH1A1* and *ALDH1A3* (encoding RALDH1 and RALDH3) were hardly expressed in $CD1c^+$ mDCs even in the presence of the indicated stimulation (Fig. 1J, 1K).

Collectively, 1) $CD1c^+$ mDCs, but not the other human blood DC subsets, express a high level of RALDH2 in response to GM-CSF plus $VD_3$, and exogenous RA augments the expression, and 2) proinflammatory factors (TLR ligands and TNF) suppress the expression of RALDH2.

### *Human $CD103^-$ mDCs in MLNs gain ALDH activity in response to the $VD_3$-containing stimulus*

To examine whether human MLN DCs exhibit ALDH activity as mouse MLN $CD103^+$ DCs do (3, 4), DC subsets were isolated from MLNs of patients with colon cancer or Crohn's disease in the same way as done for blood DCs (Supplemental Fig. 1D). Unlike in blood, $CD141^{high}$ mDCs were not identified as a discrete population in MLNs. $CD11c^{high}$ mDCs were subdivided into $CD103^+$ and $CD103^-$ mDCs. pDCs did not express CD103.

Unlike mouse MLN DCs, freshly isolated human $CD103^+$ MLN mDCs did not have ALDH activity (Fig. 2). Unexpectedly, $CD103^-$ but not $CD103^+$ MLN mDCs gained a high level of ALDH activity in response to GM-CSF, RA, and $VD_3$. pDCs did not exhibit ALDH activity. All the above results were the same in DCs from both colon cancer and Crohn's disease. Thus, in humans, $CD103^-$ but not $CD103^+$ MLN mDCs may be RA-producing DCs in situ in the intestine.

### *Mouse splenic and MLN cDCs gain ALDH activity in response to GM-CSF alone*

Genome-wide expression profiling clustered human $CD141^{high}$ mDCs and $CD1c^+$ mDCs with mouse $CD8^+$ cDCs and $CD8^-$ cDCs, respectively (18). Thus, we examined whether $VD_3$ differentially induces mouse splenic cDC subsets to gain ALDH activity. As we reported (4), GM-CSF alone was sufficient to induce high levels of ALDH activity in both $CD8^+$ DCs and $CD8^-$ DCs in the spleen (Fig. 3A). Neither RA nor $VD_3$ augmented the activity. Unlike in human $CD1c^+$ mDCs, LPS did not suppress it. There were no substantial differences in cell viability between different culture conditions (data not shown). We also examined ALDH activity in mouse MLN cDCs in the absence or presence of the $VD_3$-containing stimulus. As reported (3), fresh $CD103^+$ but not $CD103^-$ cDCs in MLNs exhibited ALDH activity (Fig. 3B). Again, GM-CSF alone was sufficient to induce high levels of ALDH activity in both $CD103^+$ and $CD103^-$ cDCs, and the addition of RA and $VD_3$ did not augment it.